# การเตรียมอนุภาคนาโนของทองจากน้ำทิ้งอุตสาหกรรมเครื่องประดับ
## โดยใช้ซิลิกาที่มีหมู่ฟังก์ชันอะมิโดอะมิดอกซีม

นางสาวณัทพัชญ์ศา ศิริกาญจนวานิช

**PREPARATION OF GOLD NANOPARTICLES FROM JEWELRY INDUSTRY WASTEWATER**

**BY AMIDO-AMIDOXIME FUNCTIONALIZED SILICA**

**Miss Nutpatsa  Sirikanjanawanit**

**A Thesis Submitted in Partial Fulfillment of the Requirements**

**for the Degree of Master of Science Program in Chemistry**

**Department of Chemistry**

**Faculty of Science**

**Chulalongkorn University**

**Academic Year 2007**

Thesis Title          PREPARATION OF GOLD NANOPARTICLES FROM
                      JEWELRY INDUSTRY WASTEWATER BY AMIDO-
                      AMIDOXIME FUNCTIONALIZED SILICA

By                    Miss Nutpatsa Sirikanjanawanit

Field of Study        Chemistry

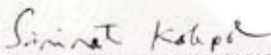Thesis Advisor        Assistant Professor Narong Praphairaksit, Ph.D.

Thesis Co-Advisor     Assistant Professor Apichat Imyim, Ph.D.

Accepted by the Faculty of Science, Chulalongkorn University in Partial
Fulfillment of the Requirements for the Master's Degree

.................................................. Dean of the Faculty of Science
(Professor Supot Hannongbua, Dr.rer.nat)
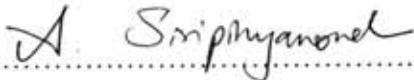
THESIS COMMITTEE

.................................................. Chairman
(Associate Professor Sirirat Kokpol, Ph.D.)

.................................................. Thesis Advisor
(Assistant Professor Narong Praphairaksit, Ph.D.)

.................................................. Thesis Co-Advisor
(Assistant Professor Apichat Imyim, Ph.D.)

.................................................. Member
(Puttaruksa Varanusupakul, Ph.D.)

.................................................. Member
(Assistant Professor Atitaya Siripinyanond, Ph.D.)

ฉัทพัชญ์ศา  ศิริกาญจนวานิช : การเตรียมอนุภาคนาโนของทองจากน้ำทิ้งอุตสาหกรรม
เครื่องประดับโดยใช้ซิลิกาที่มีหมู่ฟังก์ชันอะมิโด-อะมิดอกซีม.  (PREPARATION  OF
GOLD NANOPARTICLES FROM JEWELRY INDUSTRY WASTEWATER BY
AMIDO-AMIDOXIME FUNCTIONALIZED SILICA) อ.ที่ปรึกษา: ผศ. ดร. ณรงค์
ประไพรักษ์สิทธิ์, อ.ที่ปรึกษาร่วม: ผศ. ดร. อภิชาติ อิ่มยิ้ม, 76 หน้า.

ทำการดัดแปรสมบัติทางเคมีของซิลิกาเจลโดยการทำปฏิกิริยากับ  3-อะมิโนโพรพิลไตรเอ
ธอกซีไซเลนและเมทิลไซยาโนอะซิเตต  แล้วรีดิวซ์ด้วยไฮดรอกซีลามีน  ได้ซิลิกาเจลที่มีหมู่
ฟังก์ชันอะมิโดอะมิดอกซีม (Ami-$SiO_2$) ตรวจหาลักษณะเฉพาะของซิลิกาเจลที่สังเคราะห์ได้ด้วย
เทคนิคคาร์บอน-13 เอ็นเอ็มอาร์ การวิเคราะห์ธาตุองค์ประกอบ ฟูเรียร์ทรานสฟอร์มอินฟาเรด และ
การวิเคราะห์เชิงความร้อน ทดสอบสมบัติการรีดิวซ์ด้วยการไทเทรตกับ $KMnO_4$ พบว่า Ami-$SiO_2$
สามารถรีดิวซ์ $KMnO_4$ ได้ 1.6±0.1 มิลลิสมมูลต่อกรัมของซิลิกา นำซิลิกาที่สังเคราะห์ได้มาใช้เป็นตัว
รีดิวซ์และดูดซับคลอโรออเรตไอออนให้เป็นทองที่มีขนาดอนุภาคระดับนาโนเมตร ทำการศึกษาตัว
แปรที่มีผลต่อการเกิดอนุภาคทองระดับนาโนเมตรดังนี้ ค่าพีเอช ความเข้มข้นของสารละลายทอง
เวลาในการสัมผัส และไอออนร่วม ตรวจสอบปริมาณของทองที่เหลือในสารละลายด้วยเทคนิคเฟลม
อะตอมมิกแอบซอร์พชันสเปกโทรเมตรี ตรวจหาลักษณะเฉพาะของอนุภาคทองด้วยเทคนิคเอ็กซ์เรย์
ดิฟแฟรกโทรเมตรี, เทคนิคเอ็กซ์เรย์ฟลูออเรสเซนต์สเปกโทรเมตรี และดิฟฟิวส์รีเฟลกแทนส์
อัลตราไวโอเลตวิสิเบิลสเปกโทรเมตรี ศึกษารูปร่างและขนาดของอนุภาคทองด้วยกล้องจุลทรรศน์
อิเล็กตรอนแบบส่องผ่าน พบว่าไอออนทองในรูป $[AuCl_4]^-$ จะถูกรีดิวซ์เป็นอนุภาคทองได้ดีที่สุดที่พี
เอช 3.0 มีขนาดเฉลี่ยเท่ากับ 37±6 นาโนเมตร ความสามารถในการดูดซับและรีดิวซ์สูงสุดมีค่าเท่ากับ
39±0.1 มิลลิกรัมต่อกรัมของซิลิกา สำหรับไอออนร่วม ได้แก่ $Ag^+$, $Cu^{2+}$, $Ni^{2+}$ และ $Zn^{2+}$ ไม่ส่งผล
รบกวนการเตรียมอนุภาคทอง แต่สารละลายทองในรูป $[Au(CN)_4]^-$ จะไม่สามารถถูกรีดิวซ์ให้เป็น
อนุภาคทองขนาดนาโนเมตรได้ และได้นำภาวะที่เหมาะสมนี้ไปใช้ในการเตรียมอนุภาคทองในระดับ
นาโนเมตรจากน้ำทิ้งจากอุตสาหกรรมเครื่องประดับได้

| ภาควิชา | เคมี | ลายมือชื่อนิสิต Nutpatsa Sirikanjanawanit |
|---|---|---|
| สาขาวิชา | เคมี | ลายมือชื่ออาจารย์ที่ปรึกษา |
| ปีการศึกษา | 2550 | ลายมือชื่ออาจารย์ที่ปรึกษาร่วม |

## # # 487 22875 23 : MAJOR   CHEMISTRY

KEY WORD : MODIFIED SILICA GEL / AMIDOXIME / GOLD NANOPARTICLES / JEWELRY INDUSTRY WASTEWATER

NUTPATSA SIRIKANJANAWANIT: PREPARATION OF GOLD NANOPARTICLES FROM JEWELRY INDUSTRY WASTEWATER BY AMIDO-AMIDOXIME FUNCTIONALIZED SILICA. THESIS ADVISOR: ASST.PROF. NARONG PRAPHAIRAKSIT, Ph.D., THESIS COADVISER: ASST.PROF. APICHAT IMYIM, Ph.D., 76 pp.

Silica gel was initially modified with 3-aminopropyltriethoxysilane and methylcyanoacetate and then reduced with hydroxylamine, yielding amido-amidoxime silica (Ami-SiO$_2$). The Ami-SiO$_2$ was characterized by $^{13}$C-NMR, elemental analysis, FT-IR, and TGA techniques. A reducing capacity of $1.6\pm0.1$ mEq / g Ami-SiO$_2$ was found by titration with KMnO$_4$. Various parameters affecting gold nanoparticle formation such as pH, concentration of gold ion, contact time, co-ions were optimized. Residual gold in solution was determined by flame atomic absorption spectrometry. The characterization of gold nanoparticles were carried out by X-ray diffractometry, X-ray fluorescence spectrometry, Diffuse-reflectance ultraviolet visible spectrometry and the average particle size of gold nanoparticles of $37\pm6$ nm was estimated by transmission electron microscopy. The $[AuCl_4]^-$ solution was best reduced at pH 3.0. The maximum capacity of reduction was $39\pm0.1$ mg / g Ami-SiO$_2$. The preparation of gold nanoparticles was not affected by $Ag^+$, $Cu^{2+}$, $Ni^{2+}$ and $Zn^{2+}$. The $[Au(CN)_4]^-$ was not reduced into gold nanoparticles by the modified silica. The optimized conditions were applied for preparation of gold nanoparticles from jewelry industry wastewater.

| | | |
|---|---|---|
| Department | Chemistry | Student's signature  Nutpatsa Sirikanjanawanit |
| Field of study | Chemistry | Advisor's signature  Narong Praphairaksit |
| Academic year | 2007 | Co-advisor's signature |

# ACKNOWLEDGEMENTS

# CONTENTS

# LIST OF TABLES

# LIST OF FIGURES

# LIST OF SYMBOLS AND ABBREVIATIONS

| | |
|---|---|
| $^{13}$C-NMR | 13-Carbon nuclear magnetic resonance |
| $^{o}$C | Degree Celsius |
| DR-UV-Vis | Diffuse reflectance ultraviolet-visible spectrophotometry |
| $E^{o}$ | Standard reduction potential |
| EA | Elemental analysis |
| FAAS | Flame atomic absorption spectrometry |
| FT-IR | Fourier transform infrared spectroscopy |
| g | Gram |
| Log $\beta$ | Stability constant |
| mg L$^{-1}$ | Milligram per liter |
| mm | Millimeter |
| nm | Nanometer |
| TEM | Transmission electron microscopy |
| TGA | Thermal gravimetric analysis |
| UV-Vis | Ultraviolet-visible spectrophotometry |
| XRD | X-ray diffractometry |
| XRF | X-ray fluorescence spectrometry |
| SiO$_2$ | Silica gel |
| AP-SiO$_2$ | Aminopropyltriethoxysilane functionalized silica |
| CA-SiO$_2$ | Cyano-amido functionalized silica |
| Ami-SiO$_2$ | Amido-amidoxime functionalized silica |

# CHAPTER I

# INTRODUCTION

## 1.1 Statement of the problem

Gold is an invaluable metal, especially in economic aspect. Due largely to its reflectivity, high corrosion resistance, and high electrical conductivity; gold is mainly used in jewelry, electronic devices, and dentistry [1]. Nowadays, gold can be further applied in nanotechnology. As the particle size of gold decreased to nanometer level its property changes significantly, creating many more applications and advantages. For example, gold nanoparticles can be used as a drug delivery system [2], electrochemical sensors [3], and catalyst [4]. There are three established methods to prepare gold nanoparticles, i.e. chemical reduction, photoreduction, and on-solid reduction. In photoreduction, light is used in order to reduce gold ions but it takes long time to complete the reduction. In addition, both of the first two methods also need a solid support to stabilize gold nanoparticles and prevent the agglomeration of nanoparticles after the reduction. The agglomeration will create bigger particles and its chemical properties will be changed. The third method is to use a reducing functional group moiety on a solid support that is able to reduce gold ions into gold nanoparticles. This makes it easy to use due to the fact that the reduction of gold ions and the binding of gold nanoparticles occur simultaneously. By the way, the selection of the solid support used in each process depends on what kind of application of gold nanoparticle is going to be used.

Moreover, for the on-solid reduction method, the functional groups that are able to reduce gold ions can act as an extractant of gold ions from wastewater resulted from manufacture and transformation of jewelry industry where large amounts of gold

are used. The advantage of this method is simplicity and a shorter time compared to Wohlwill electrolytic process and Fizzer cell process [5].

Several studies have reported various materials for the preparation of gold nanoparticles i.e. polymer, clay, silica. Among them, silica is non-toxic and its surface is easy to modify because of high silanol-containing surface area. However, the reduction of gold ions requires a reducing group. Amidoxime functional group was chosen in this research due to its reducing-adsorption capacity and selectivity towards Au(III) ion [6].

In this work, silica was functionalized with amido-amidoxime functional group and used to study the optimized condition and applied for the preparation of gold nanoparticles from real wastewater sample.

## 1.2 Scope of the research

The scope of this research is the synthesis and characterization of amido-amidoxime functionalized silica. Then the synthesized silica is brought to find suitable condition for the reduction of gold ions into gold nanoparticles by batch method and to study the following parameters: i.e. the effect of pH of gold solution, the effect of concentration of gold, the contact time, the effect of metal ion interferences ($Ag^+$, $Cu^{2+}$, $Ni^{2+}$, and $Zn^{2+}$). Two types of gold solution to be evaluated are $[AuCl_4]^-$ and $[Au(CN)_4]^-$. First, $[AuCl_4]^-$ is studied with every parameters mentioned above. Then the suitable condition is used to perform with $[Au(CN)_4]^-$ and applied to real wastewater sample. Gold complex in real wastewater sample was chloroaurate.

## 1.3  The benefits of this research

The amido-amidoxime functionalized silica (Ami-SiO$_2$) can be used to prepare gold nanoparticles from jewelry industry wastewater.

# CHAPTER II

# THEORY AND LITERATURE REVIEW

## 2.1    Properties of gold

Gold is an invaluable metal that is generally found in nature as metallic gold and gold compounds. It was known that gold can occur in one of six oxidation states, from -1 to +5 [7]. Both metallic gold and gold compounds were useful in several aspects.

### 2.1.1   Metallic gold

Metallic gold is a metal that is not oxidized in air (even at high temperatures) or water by either oxygen or sulfur, and is not attacked under the most corrosive conditions [8].

#### 2.1.1.1   Bulk gold

Bulk gold has a yellow color and bright luster. It is a soft and ductile metal and is usually alloyed to strengthen it. In addition, bulk gold has a melting point at $1064^{o}$C [9], and has face center cubic (fcc) structure which exhibits highly symmetry. Bulk gold is in cubic, octahedral or rhombododecahedral crystal forms [10]. It has high conductivity and electrical properties leading to widespread use in modern industry.

#### 2.1.1.2   Gold in nanoscale

The color of gold nanoparticles may range from red through purple to blue and almost black. This is due to a change in their absorption spectrum on the formation of aggregates. A melting point of gold nanoparticle is shrunken from that of bulk gold. The reason for this phenomenon is the huge increase in surface area of gold

nanoparticles. From the calculations of Liu et al. [11] and measurements of Dick et al. [12], they indicated that gold nanoparticles in a 5 nm size range would melt at about $830^{\circ}$C, particles of about 2 nm would liquefy at $350^{\circ}$C. These results are shown in Figure 2.1.
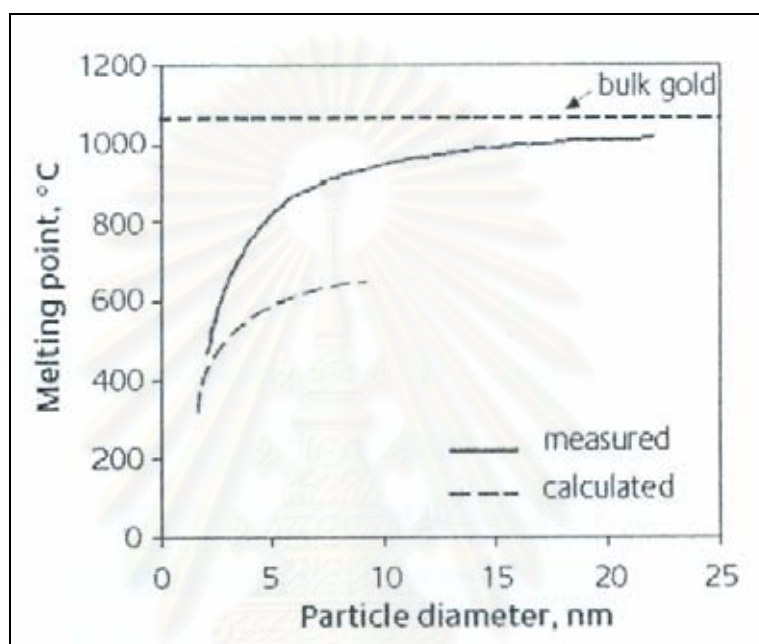


**Figure 2.1**  Melting points of gold nanoparticles as a function of particle diameter.

The crystalline structure of gold at the nanoscale differs from the bulk one. Several attempts have been made to predict the structure of gold nanoparticles by calculation. In general, the results from calculations are not completely in agreement, either with each other or with the results of experimental techniques. Some shapes of gold nanoparticles are shown in Figure 2.2 [13]. The surface plasmon band (SPB) of gold nanoparticle is a characteristic electronic property which exhibits a broad absorption band in the visible region around 520 nm due to the crystalline structure of gold nanoparticle. The SPB is the result from the collective oscillation of the electron cloud at the surface of nanoparticles that is correlated with the electromagnetic field of the incoming light.
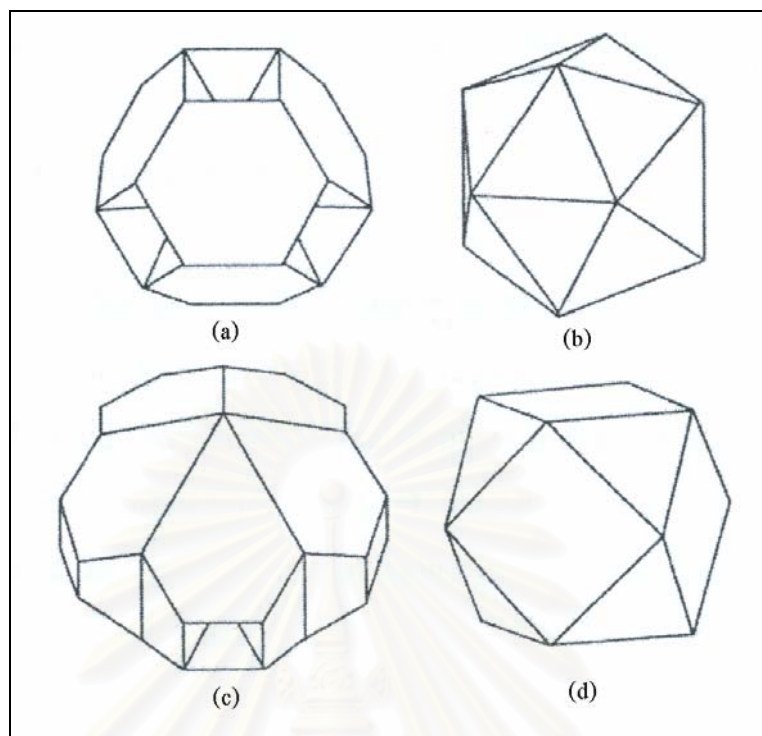
**Figure 2.2** Some shapes of gold nanoparticles (a) truncated octahedron,

(b) icosahedron, (c) Marks decahedron and (d) cuboctahedron [13].

### 2.1.2 Gold compounds

Gold compounds in natural state are tellurides ($AuTe_2$) and stibnites ($AuSb_2$). Gold is almost invariably associated with quartz or pyrite, both in veins and in alluvial or placer deposits [14]. The metallic gold is dissolved by combined process of oxidation and complexation. In the presence of a complexing ligand, aurous (Au(I)) or auric (Au(III)) cations will form stable complexes or be further reduced by water to metallic gold [15]. The coordination numbers of Au(I) and Au(III) are 2 and 4 tending to form linear and square planar complexes, respectively. Some of these complexes are listed in Table 2.1 with their stability constants (log β) and standard reduction potentials ($E^o$) of the corresponding reduction reactions.

**Table 2.1**   Stability constants for selected Au(I) and Au(III) complexes and standard reduction potentials

| Complex | Log β | Reduction Reaction | $E^o$ (V) | Ref |
|---|---|---|---|---|
| - | - | $Au^+ + e^- = Au$ | 1.69 | 15 |
| $Au(CN)_2^-$ | 38.3 | $Au(CN)_2^- + e^- = Au + 2CN^-$ | -0.57 | 15 |
| $Au_2(HS)_2S^{2-}$ | 72.9 | $Au_2(HS)_2S^{2-} + 2e^- = 2Au + S^{2-} + 2HS^-$ | -0.47 | 17 |
| $AuS^-$ | 36.3 | $AuS^- + e^- = Au + S^{2-}$ | -0.46 | 16 |
| $Au(HS)_2^-$ | 32.8 | $Au(HS)_2^- + e^- = Au + 2HS^-$ | -0.25 | 17 |
| $Au(SO_3)_2^{3-}$ | 26.8 | $Au(SO_3)_2^{3-} + e^- = Au + 2SO_3^{2-}$ | 0.11 | 17 |
| $Au(S_2O_3)_2^{3-}$ | 26.0 | $Au(S_2O_3)_2^{3-} + e^- = Au + 2S_2O_3^{2-}$ | 0.15 | 16 |
| $Au(CSe(NH_2)_2)_2^+$ | 25.3 | $Au(CSe(NH_2)_2)_2^+ + e^- = Au + 2CSe(NH_2)_2$ | 0.20 | 16 |
| $Au(CS(NH_2)_2)_2^+$ | 22.0 | $Au(CS(NH_2)_2)_2^+ + e^- = Au + 2CS(NH_2)_2$ | 0.38 | 16 |
| $Au(NH_3)_2^+$ | 19.0 | $Au(NH_3)_2^+ + e^- = Au + 2NH_3$ | 0.57 | 16 |
| $AuI_2^-$ | 19.0 | $AuI_2^- + e^- = Au + 2I^-$ | 0.57 | 16 |
| $Au(SCN)_2^-$ | 17.1 | $Au(SCN)_2^- + e^- = Au + 2SCN^-$ | 0.66 | 15 |
| $AuBr_2^-$ | 12.0 | $AuBr_2^- + e^- = Au + 2Br^-$ | 0.98 | 15 |
| $AuCl_2^-$ | 9.0 | $AuCl_2^- + e^- = Au + 2Cl^-$ | 1.16 | 16 |
| - | - | $Au^{3+} + 3e^- = Au$ | 1.50 | 15 |
| $Au(CN)_4^-$ | ~56 | $Au(CN)_4^- + 3e^- = Au + 4CN^-$ | 0.40 | 15 |
| $Au(NH_3)_4^{3+}$ | ~59 | $Au(NH_3)_4^{3+} + 3e^- = Au + 4NH_3$ | 0.33 | 18-19 |
| $AuI_4^-$ | 47.7 | $AuI_4^- + 3e^- = Au + 4I^-$ | 0.56 | 15 |
| $Au(SCN)_4^-$ | 42 | $Au(SCN)_4^- + 3e^- = Au + 4SCN^-$ | 0.62 | 15 |
| $AuBr_4^-$ | 32 | $AuBr_4^- + 3e^- = Au + 4Br^-$ | 0.87 | 15 |
| $AuCl_4^-$ | 26 | $AuCl_4^- + 3e^- = Au + 4Cl^-$ | 1.00 | 15 |

## 2.2    Preparation of gold nanoparticles

The preparation of gold nanoparticles has received considerable attention due to their interesting application. Gold nanoparticles could be synthesized in aqueous solution by the chemical reduction. However, the chemical reduction concerned the reduction potential value ($E^o$). Moreover, gold nanoparticles could be also prepared by photoreduction or photochemical reaction.

### 2.2.1    Chemical reduction

Gold nanoparticles can be formed by using some special  substances present in both solid and solution forms. The reaction between the substances and Au(III) is often a redox reaction which changes the oxidation state of gold from 3 to 0 (gold nanoparticle). Two main chemical reduction processes are summarized as follows.

#### 2.2.1.1   Use of reducing agents

The reducing agents have been utilized for the reduction of Au(III) to gold nanoparticles. Typical reducing agents for the preparation of gold nanoparticles are $NaBH_4$ [20], citrate salts [21], ascorbic acid [22], and hydroxylamine [23].

#### (a)   Citrate reduction

This method involves the reduction of $HAuCl_4$ in water, which was introduced by Turkevitch in 1951 [24]. Sodium citrate firstly acts as a reducing agent. Afterward, the negatively charged citrate ions are adsorbed onto the gold nanoparticles and leading to the surface change that repels the particles and prevents them from aggregation. This method is often used even now when a rather loose shell of ligand are required around the gold core in order to prepare a precursor to valuable gold nanoparticle-based materials [25].

#### (b)   The Brust-Schiffrin method

Mulvaney and Giersig reported the stabilization method of gold nanoparticles in 1993 by using thiols of different chain lengths. This method was called the Brust-

Schiffrin method, published in 1994 [26]. The technique of synthesis is a use of thiol ligands that strongly bind to gold due to the soft character of both Au and S [26, 27]. In a two-phase reaction system, $AuCl_4^-$ from aqueous phase is transferred to toluene phase using tetra-n-octylammonium bromide (TOAB) as the phase-transfer reagent and reduced by $NaBH_4$ forming nanoparticles that are weakly stabilized by tetra-n-octylammonium bromide which is instantaneously replaced by thiol molecules.

### 2.2.1.2 On solid reduction

An on-solid reduction method is a method that involves the reduction of Au(III) by a solid containing reducing functional group. A solid support functionalized with a reducing group was investigated by Lin et al [6]. They functionalized polyacrylonitrile (PAN) with amidoxime group and then this product was subject to reduce Au(III) into gold nanoparticles. In addition, the advantages of amidoxime group on solid support are that (i) there is an adsorption of gold nanoparticles, (ii) the solid support acts as the stabilizer for preventing of agglomeration of gold nanoparticles and (iii) the preparation step of nanogold was shortened.

### 2.2.2 Photoreduction (photochemical)

In this method, light source is used for the synthesis of gold nanoparticles. However, it is not as widespread as the chemical reduction method, due to time required but it presents advantages that the controlled reduction of metal ions can be carried out without using excess reducing agent, and no adsorbing contamination on the product occurs in the preparation process. Moreover, the radiation is absorbed regardless of the presence of light-absorbing solutes and products and the reduction reaction arises uniformly in the solution. Moriguchi et al. [28] used dioctadecyldimethylammonium chloride ($DODMA^+Cl^-$) to form complex with $AuCl_4^-$. The $DODMA^+AuCl_4^-$ complex was produced and exposed to UV-light for the preparation of gold nanoparticles. This photoreduction process lasted 12 hours.

## 2.3 Application of gold nanoparticles

The properties of gold nanoparticles are ensuring that gold is a candidate material for nanotechnology applications in the diverse areas of electronics, catalysis, biomedical and coating.

### 2.3.1 Electronics

Gold is an indispensable element for nanoscale electronic components because of its resistance to oxidation and its mechanical robustness. By comparison with other metals, only silver and platinum offer similar properties, but silver can be too reactive and platinum is significantly more expensive than gold. Hermanson et al. [29] have shown that a new class of microwires can be assembled by dielectrophoresis from suspensions of gold nanoparticles. These researchers have developed new self-assembling and repairing gold microwires. They used tiny particles of gold suspended in an aqueous solution. When electrodes were inserted into the suspension, gold wires more than 5 mm in length could be formed. It has been shown that these wires can be used as microscopic sensors for certain chemicals, such as thiol and cyanide. The principle of making electrical connections, by assembling rudimentary circuits using this technique has been established.

### 2.3.2 Catalyst

Recently gold is used as a catalyst in chemical processing. In the field of selective oxidation, Dow Chemical Company has patented the selective production of propene oxide by the epoxidation of propene in the presence of hydrogen and gold on $TiO_2/SiO_2$ catalyst [30]. Gold nanoparticles have been used in pollution control and fuel cell. The basis of fuel cell energy generation is believed that there are significant opportunities for gold catalysts in automotive industry [31]. The automotive systems for using gold nanoparticles are shown in Table 2.2. The ability of gold to oxidize CO

and remove $NO_x$ compounds offers scope for air quality improvement and control of malodors. They can apply in buildings, transport or other applications.

**Table 2.2** Potential areas within automotive systems for using nanoparticulated gold catalysts

| Automotive Power Source | Application for Gold Based Catalysts | Reaction (s) | Main Characteristic of Supports Gold Nanoparticulate Catalyst |
|---|---|---|---|
| Fuel cell | Fuel processing System for clean $H_2$ production | Water gas shift reaction for $H_2$ production | High activity at low Temperature |
| | | Preferential oxidation of CO for $H_2$ clean up | High activity at low Temperature |
| | | Methanol decomposition for $H_2$ production | High activity |
| | Fuel cell catalyst | Oxidation removal of CO From $H_2$ | Improvement in electrical conductivity |
| Diesel Engine | Component of TWC For diesel engine Emission control | CO and HC Combustion and $NO_x$ reduction HC | Low temperature activity (and high for $NO_x$ reduction) |
| Petrol Engine | Low light off catalyst For petrol engine | CO and HC combustion | Low temperature activity |

### 2.3.3 Biomedical

The current and potential applications of gold in the biomedical sector are highlighted below, classified by the form in which the gold is employed (bulk gold, gold nanoparticles and gold compounds) in Table 2.3. Gold is used in dental alloys and in inner ear implants and coatings for patients. Gold also plays a role in targeted drug delivery through the 'pharmacy on a chip' concept, where gold coated microcapsules of drugs are controllably released intravenously into the body. For gold nanotechnology, the current applications in sensing and labeling are being joined by emerging applications in the targeted destruction of cancer cells. Gold compounds

already were used in drugs related to the treatment of arthritis. Moreover, it can be effective in the treatment of some types of cancer [32].

**Table 2.3** Current and emerging uses of gold in biomedical applications

|  | Bulk gold / alloys | Gold nanoparticle | Gold compound |
|---|---|---|---|
| Dental Alloys | C | | |
| Prothesis / implants | C | | |
| Stents | C | | |
| Sensors / Labeling | | C | |
| Drug Delivery | E | P | |
| Arthritis Treatment | | | C |
| Cancer Treatment | | P | E |
| Anti-bacterial | P | P | P |

C = Current application, E = Emerging application and P = Possible application

### 2.3.4 Coating

Colloidal gold has long been the basis of decorative effects in glass and tableware because colloidal gold has red to dark purple colors. Recently, Nippon Paint has introduced a new stabilized polymer using gold nanoparticle-containing paint. This has novel dynamic optical effects, changing color, depending on the external lighting conditions [33]. It is interesting to consider other applications for decorative effects.

## 2.4 Characterization of nanogold and determination of gold content

Gold ions or gold complexes are always present in liquid phase, especially in aqueous solution. They are usually determined by atomic spectrometry. While gold nanoparticles are characterized by different techniques such as diffuse reflectance ultraviolet spectrophotometry (DR-UV-Vis), X-ray diffractometry (XRD), and transmission electron microscopy (TEM).

### 2.4.1 Flame atomic absorption spectrometry (FAAS) [34]

Atomic absorption spectrometry is used for the analysis and characterization of the elemental composition of materials and samples. When the sample is atomized by flame, a substantial fraction of the metallic constituents are reduced to gaseous atoms. In flame atomization, a solution of the sample is sprayed into a flame by means of a nebulizer. The high temperature causes formation of atoms which can be observed by absorption spectroscopy. A block diagram of an atomic absorption spectrometer is shown in Figure 2.3.
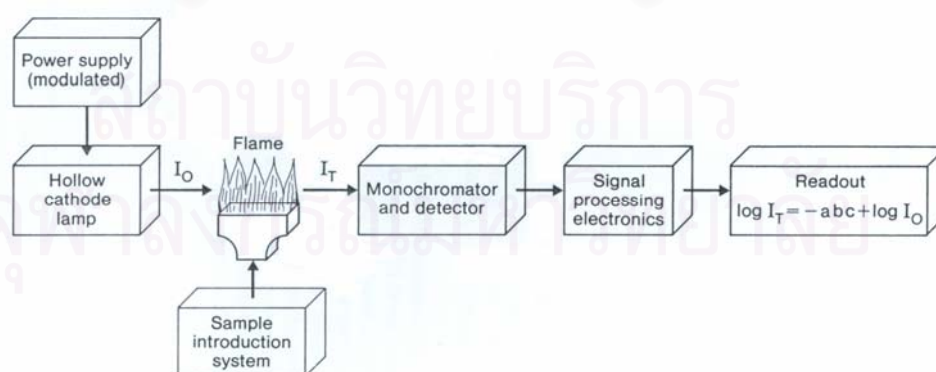


**Figure 2.3** Block diagram of an atomic absorption spectrometer.

## 2.4.2 Diffuse reflectance ultraviolet spectrophotometry (DR-UV-Vis) [35]

The diffuse reflectance was used for purposes involving light absorbing and reflecting materials. The radiation penetrates the surface layer of the sample and excites vibrational modes of the analyte molecule, and is then scattered in all directions. A schematic of an instrument is shown in Figure 2.4.
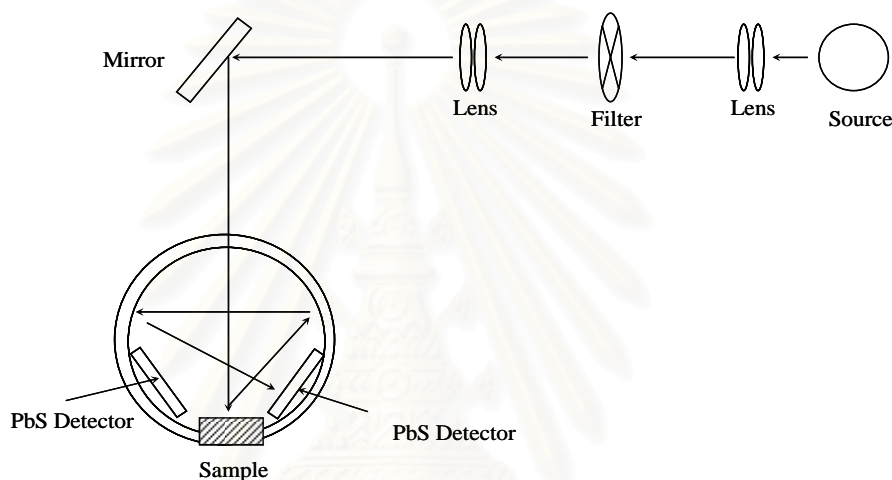


**Figure 2.4** The schematic of DR-UV-Visible spectrometer.

The radiation source is usually a tungsten lamp to provide adequate continuum radiation over the entire visible region. $D_2$ or $H_2$ lamp is required which have radiation in range of 160-360 nm. A sample is packed on a holder sample and irradiated. After that light intensity is magnified with lens and detected by a detector. The interior wall of the holder sample may be coated for a nearly perfect diffuse reflectance material such as barium sulfate. Radiation reflected from the sample ultimately reaches the detectors after multiple reflections off the walls of the sample holder by using the tilting mirror which permits a measurement of the ratio of the intensity of the radiation reflected from the sample and that reflected off the wall. The absorption and scattering of completely diffuse monochromatic radiation by a homogeneous isotropic light

scattering layer was evaluated by using Schuster-Kubelka-Munk theory. The formula is determined from the resulting Kubelka-Munk function. The absorption is calculated from the equation (2.4.2).

$$F(R_\infty) \;=\; (1-R_\infty)^2 / (2R_\infty) \tag{2.4.2}$$

where  $R_\infty$ is the diffuse reflectance from a semi-infinite layer

and      $F(R_\infty)$ is an absorbance proportional to the absorption coefficient

### 2.4.3  X-ray diffractometry (XRD) [36]

When an X-ray beam strikes a surface of crystalline sample at an angle $\theta$, a portion of the radiation is scattered by the layer of atoms at the surface. The effect of scattering from the regularly spaced centers of the crystal is a diffraction of the beam. The data of X-ray diffraction indicates that the spacing between layers of atoms and the scattering centers must be spatially distributed in a higher regular way. The diffraction of X-rays by crystals is shown in Figure 2.5.
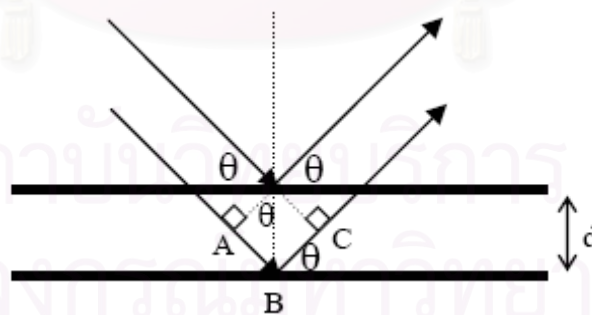


**Figure 2.5**  Diffraction of X-rays by a crystal.

A narrow beam strikes the crystal surface at angle $\theta$; scattering occurs as a consequence of interaction of the radiation with atoms located at B. The distance was calculated from formula (2.1).

$$AB \; + \; BC \;\; = \;\; \mathbf{n}\lambda \tag{2.1}$$

The scattered radiation will be in phase, and the crystal will appear to reflect the X-radiation. It is investigated with formula (2.2).

$$AB \; = \; BC \;\; = \;\; d \sin\theta \tag{2.2}$$

Thus the condition for constructive interference of the beam at angle $\theta$ is expressed by the formula (2.3), called Bragg's law.

$$2d \sin\theta \;\; = \;\; \mathbf{n}\lambda \qquad \textbf{Bragg's law} \tag{2.3}$$

where    $\mathbf{n}$ = an integer

          d = interplanar distance of the crystal (Å ; 1 Å = $10^{-10}$ m)

          $\theta$ = angle between X-ray and crystal planes (degree)

          $\lambda$ = wavelength (Å)

### 2.4.4 X-ray fluorescence spectrometry (XRF) [34]

An X-radiation (fluorescence) emission of each element is detected in XRF technique. There are two ways for the detection of the fluorescence intensity or energy, i.e. wavelength dispersive (WDX) and energy dispersive (EDX) techniques. In EDX, the energy of a characteristic X-ray is adapted by a detector and output data reports in the relative of intensity and electron volt (eV). An energy dispersive XRF spectrometer diagram is shown in Figure 2.6.
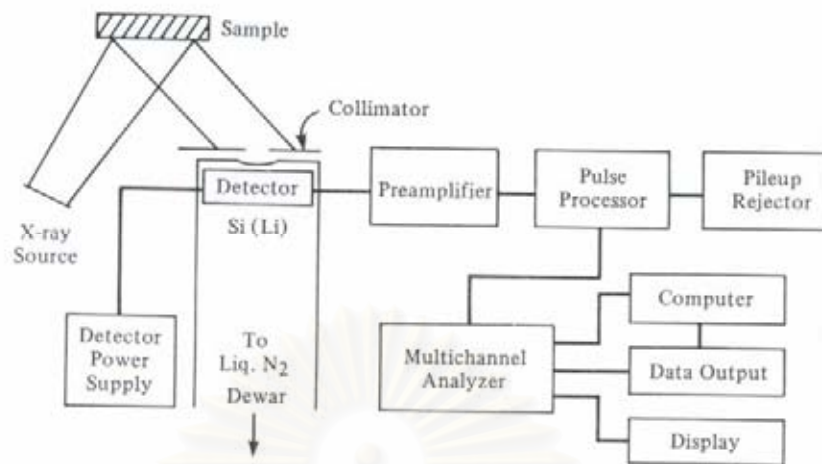
**Figure 2.6** Energy dispersive X-ray fluorescence spectrometer.

### 2.4.5 Transmission electron microscopy (TEM) [35]

A schematic TEM instrument is shown in Figure 2.7. High energy electron beam passes through a condenser lens to produce parallel rays, which affect the sample. The transmitted beam represents a two-dimensional image of the sample which is subsequently magnified by electron optics. It produces a so-called bright field image. Typical operating conditions of a TEM instrument are 100-200 keV, $10^{-6}$ mbar vacuum, 1 nm resolution and a magnification of $10^{5}$ to $10^{6}$.
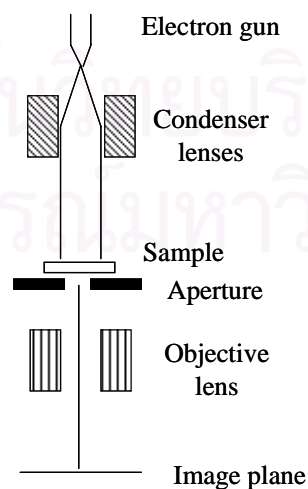


**Figure 2.7** Schematic diagram of transmission electron microscope.

Furthermore, TEM technique is used to determine particles size of gold nanoparticles. The reduced gold nanoparticles have a broad distribution of size and shapes. An average particle size can be calculated by a formula (2.4.3) [37].

$$d_s \quad = \quad \sum n_i d_i^3 \ / \ \sum n_i d_i^2 \qquad (2.4.3)$$

where  $d_s$ = the average particle diameter

$d_i$ = particle diameter

$n_i$ = amount particle

## 2.5 Literature review

Metallic gold, either in the form of bulk gold or as nanoparticles, are widely used in many fields of nanotechnology such as drug delivery and sensor. Gold nanoparticles are suitable for drug delivery because the therapeutic agent can be attached on the surface of gold nanoparticles which are non-toxic and can direct penetrate into the cytoplasm or nucleus of the target cell [38]. Yang et al. [39] studies the preliminary drug-carrying experiment of gold nanoparticles. The result showed that the gold nanoparticles could successfully carry anti-tumor drug [$cis$-Pt(NH$_3$)$_2$Cl$_2$] and possess potential for drug delivery applications. In the field of electrochemical sensor, gold nanoparticles have received considerable attention due to their relative high surface area-to-volume ratio, which significantly differ from their bulk counterparts. Thus, nanogold modified electrochemical interface behaving as nanoelectrode assembles have been widely used for enhancing catalytic interface for the development of electrochemical sensors. Raj et al. [3] modified the surface of gold working electrode with 1,4-benzenedimethanetiol. The modified electrode was coated with gold nanoparticles, thereby its active sites can facilitate the electron transfer for the reduction of oxygen. It was found that the gold nanoparticles achieve good electrical communication with the underlying electrode surface and efficiently catalyze the reduction of oxygen.

The preparation of gold nanoparticles can be conducted by various methodologies such as the use of reducing agents and photoreduction, i.e. using light for the controlled reduction of gold ions. However, these two methods require the use of stabilizers to prevent the aggregation of gold nanoparticles. Brust et al. [26] reduced Au(III) into gold nanoparticles by using NaBH$_4$ and used thiol molecules as the stabilizer. Ghosh et al. [40] modified mesoporous silica with amine (-NH$_2$) and thiol (-SH) functional groups for the adsorption of gold nanoparticles obtained from the photoreduction method. Moreover, gold nanoparticles were prepared by using on-solid

reduction method that is a modification of reducing functional group on a material surface. The reducing functional group can adsorb and reduce Au(III) in solution into gold nanoparticle on the support surface. The advantages of this method are that it is flexible to choose the solid support for the modification of reducing functional group (e.g. alumina [41], silica, charcoal, and clay [42]) and the preparation step of gold nanoparticles was shortened. For instance, amidoxime functional group was modified on polyacrylonitrile (PAN) as shown in Figure 2.8, by Lin et al. [6]. As a result, amidoxime functional group can reduce Au(III) into gold nanoparticles.

$$P—C{=}N—OH$$
$$\underset{\displaystyle NH_2}{|}$$
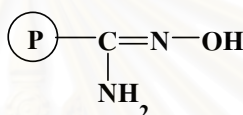
**Figure 2.8**  Structure of amidoxime functionalized polyacrylonitrile.

There are various support materials that can be used for the modification. One of which that caught our interest is silica because it is cheap, durable and easy to modify. Several researches have modified silica surface with organic moieties. Evangelista et al. [43] and Padilha et al. [44] have studied the modification of silica surface with 2-mercaptothiazoline and 5-amino-1,3,4-thaidiazole-2-thiol, respectively for mercury(II) removal. In addition, Fan et al. [45] and Xie et al. [46] modified the silica surface with diphenylcarbazone and gallic acid for extraction of metals ions.

Due to the advantages of silica together with the reducing ability of amidoxime, the modification of silica surface by amidoxime functional group for the preparation of gold nanoparticles is the main interest to this study. The modification of silica surface with amidoxime through amido group (Figure 2.9) was recently reported by Ngeontae [47] in which the modified support was used successfully for the preconcentration of $Cu^{2+}$, $Co^{2+}$, $Cd^{2+}$, $Ni^{2+}$ and $Pb^{2+}$. This research will focus on the study of factors affecting the formation of gold nanoparticles by the amidoxime

functionalized silica and the potential of this technique in the preparation of gold nanoparticles from jewelry related industrial wastewater.
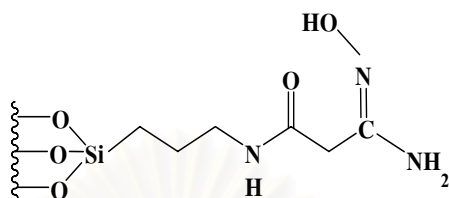


**Figure 2.9** Structure of amido-amidoxime functionalized silica.

# CHAPTER III

# EXPERIMENTAL

## 3.1 Analytical instruments

The instruments used in this study were listed in Table 3.1.

**Table 3.1** Analytical instruments

| Analytical instruments *and Model (Manufacturer)* | Purpose |
|---|---|
| 1. 13-Carbon nuclear magnetic resonance spectrometer ($^{13}$C-NMR) *Spectrum GX (Perkin-Elmer)* | Provide insights into the chemical structure of organic on solids |
| 2. CHNS/O analyzer *PE 2400 Series II (Perkin-Elmer)* | The percentage determination of carbon, nitrogen and oxygen of organic compounds |
| 3. Fourier transform infrared spectrometer (FT-IR) *Impact 410 (Nicolet)* | Characterization of functional groups |
| 4. Thermal Analyzer (TGA) *409 (Netzsch)* | Measurement of weight loss of substances deposited on silica by thermal analysis |
| 5. Flame atomic absorption spectrometer (FAAS) *AAnalyst 100 (Perkin-Elmer)* | Elemental analysis (operating parameters are shown in table 3.2) |
| 6. X-ray diffractometer (XRD) *DMAX 2200/Ultima+ (Rigaku)* | Pattern crystallites analysis |

**Table 3.1**  Analytical instruments lists (continued)

| Analytical instruments *and Model (Manufacture)* | Purpose |
|---|---|
| 7.  Diffuse reflectance ultraviolet visible spectrophotometer (DR-UV-Vis) *UV-2500PC (Shimadzu)* | Absorbance measurement for solid sample |
| 8.  UV-Vis spectrophotometer *HP 8453 (Hewllet Packard)* | Absorbance measurement |
| 9.  Transmission electron microscope (TEM) *JEM-2001* | Particle size analysis of gold nanoparticle |
| 10.  X-ray fluorescence spectrometer (XRF) *Midex ( Spectro)* | Elemental analysis on silica |
| 11.  pH meter *pH 211 (Hanna instruments)* | pH measurement |

**Table 3.2**  Operating parameters for FAAS

| **Operating conditions** | **Au** | **Ag** | **Cu** | **Ni** | **Zn** |
|---|---|---|---|---|---|
| Wavelength (nm) | 242.8 | 328.1 | 324.8 | 232.0 | 213.9 |
| Slit width (nm) | 0.70 | 0.70 | 0.70 | 0.20 | 0.70 |
| Lamp current (mA) | 15 | 15 | 15 | 25 | 15 |
| $C_2H_2$ flow-rate (L min$^{-1}$) | 3 | 3 | 3 | 3 | 3 |
| Air flow-rate (L min$^{-1}$) | 10 | 10 | 10 | 10 | 10 |

## 3.2   Chemicals

### 3.2.1   Chemicals

All chemicals used were of analytical grade and commercially available from the suppliers listed in Table 3.3.

**Table 3.3**   Chemical list

| Chemicals | Suppliers |
|---|---|
| (3-aminopropyl) triethoxysilane | Fluka |
| Barium sulfate | Wako |
| Calcium hydride | Fluka |
| Copper (II) chloride 2-hydrate | BDH |
| Dichloromethane (commercial grade) | ZEN POINT |
| Ethanol | MERCK |
| Ethanol (commercial grade) | U&V |
| Hydrochloric acid 37% | MERCK |
| Hydrogenperoxide | Fisher Scientific |
| Hydroxylammonium chloride | MERCK |
| Methyl cyanoacetate | Fluka |
| Nickel (II) chloride 6-hydrate | BDH |
| Nitric acid 65% | MERCK |
| Potassium hydroxide | MERCK |
| Potassium permanganate | MERCK |
| Silica gel (60 mesh) | MERCK |
| Silver (I) nitrate | BDH |

| Chemicals | Supplier |
|-----------|----------|
| Single element standard solution for Au(III) (1000 mg $L^{-1}$) | Fisher Scientific |
| Single element standard solution for Ag(I), Cu(II), Ni(II) and Zn(II) (1000 mg $L^{-1}$) | BDH |
| Sodium hydroxide | MERCK |
| Sodium oxalate | BDH |
| Sulfuric acid 95-97% | MERCK |
| Toluene | Fisher Scientific |
| Zinc (II) chloride | BDH |

### 3.2.2 Reagents

**(a) Aqua regia solution**

The aqua regia was prepared by mixing conc. HCl and conc. $HNO_3$ at the ratio of 3:1 v/v.

**(b) Dried toluene solution**

Toluene and calcium hydride were added to 1000 mL two-neck round bottom flask and refluxed under nitrogen atmosphere for 4 hours.

**(c) Hydrochloric acid solutions**

Hydrochloric acid (1% v/v, 5% v/v and 1 M) for pH adjustment were prepared by subsequent dilutions from the concentrated solution.

**(d) Sodium hydroxide solution**

Sodium hydroxide solution (1 M) for pH adjustment of hydroxylamine solution was prepared by dissolving the appropriate amount of NaOH in DI water.

**(e) Potassium hydroxide solution**

Potassium hydroxide solutions (1% w/v, 5% w/v and 1M) for pH adjustment were prepared by dissolving the appropriate amount of KOH in DI water.

**(f) Potassium cyanide solution**

Potassium cyanide (1 M) for complexation with Au(III) was prepared by dissolving the appropriate amount of KCN in DI water (adjusted to pH 11 to prevent the formation of toxic HCN).

**(g) Au(III) cyanide solutions $[Au(CN)_4]^-$**

40 mg/L of Au(III) chloride solutions $[AuCl_4]^-$ was adjusted to pH 7, then excess amount of KCN were added and the solution was brought to pH 3 and 10.5 to resemble acidic and basic wastes respectively.

**(h)   Interfering ions solutions**

Interfering ions solutions of $Ag^+$, $Cu^{2+}$, $Ni^{2+}$ and $Zn^{2+}$ (1000 mgL$^{-1}$) were prepared by dissolving in DI water the appropriate amount of $AgNO_3$, $CuCl_2.2H_2O$, $NiCl_2.6H_2O$ and $ZnCl_2$ respectively.

**(i)   Sodium oxalate solution**

Sodium oxalate (1.5 mM) for standardization of $KMnO_4$ was prepared by dissolving the appropriate amount of $Na_2C_2O_4$ in DI water.

**(j)   Sulfuric acid solution**

Sulfuric acid solution (2 F) for use in standardization method of potassium permanganate was prepared by dilution from the concentrated solution.

**(k)   Potassium permanganate solution**

Potassium permanganate solution (1mM) was prepared by dissolving the appropriate amount of $KMnO_4$ in DI water and standardized with sodium oxalate.

**The standardization method of potassium permanganate [48].**

25 mL of 1.5 mM sodium oxalate solution was mixed with 75 mL of 2.0 F $H_2SO_4$ and 50 mL DI water in 250 mL erlenmeyer flask. The mixture was titrated with 1mM $KMnO_4$ until light pink solution was observed. Then, the solution is heated to approximately 50-60$^o$C until the color disappear. The titration was then continued until the light pink color re-appeared and remained for at least 30 seconds.

## 3.3    Synthesis of amido-amidoxime functionalized silica

Silica gel (25 g) in a 250 mL two-neck round bottom flask was refluxed with dried toluene (150 mL) at 90-100$^o$C and stirred under nitrogen atmosphere. After 1 hour, (3-aminopropyl)triethoxysilane (10 mL) was added and the mixture was refluxed and stirred under nitrogen atmosphere for 24 hours. The solid was filtered and washed with dichloromethane (200 mL 3 times). The product, designated as AP-SiO$_2$, was refluxed with dried toluene (150 mL) at 90-100$^o$C in a 250 mL two-neck round bottom flask and stirred under nitrogen atmosphere. After 1 hour, methyl cyanoacetate (6.2 g) was added. The mixture was refluxed and stirred under nitrogen atmosphere for 24 hours. The solid was filtered and washed with ethanol (100 mL 3 times) and dichloromethane (200 mL 2 times). The product, designated as CA-SiO$_2$, was then transfered to 250 mL two-neck round bottom flask and were added ethanol (75 mL) and hydroxylamine solution [prepared by mixing hydroxylamine hydrochloride (4.6 g) with sodium hydroxide (2.7 g) in DI water (75 mL) and adjusted to pH 7 with 1M HCl and 1M NaOH]. The mixture was again refluxed and stirred under nitrogen atmosphere for 24 hours at 78$^o$C. The solid was filtered, washed with distilled water (200 mL 3 times), ethanol (200 mL 2 times), and dichloromethane (200 mL 3 times). The final product was amido-amidoxime silica (Ami-SiO$_2$) which was kept in desicator [47]. The synthetic pathway of Ami-SiO$_2$ is shown in Figure 3.1
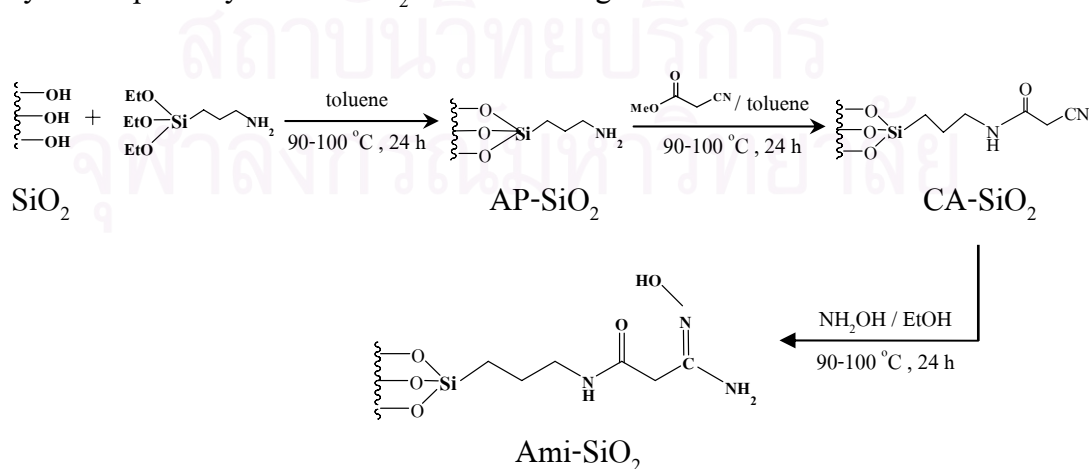


**Figure 3.1** The synthetic pathway of Ami-SiO$_2$.

## 3.4    Characterization of silica

The functionalized silica was characterized with $^{13}$C-NMR, FT-IR, EA and TGA techniques.

### Carbon nuclear magnetic resonance spectrometer ($^{13}$C-NMR)

$^{13}$C-NMR is an analytical technique that indicates the various carbon sites on the solid. The carbon site shows in term of chemical-shift ranges.

### Fourier transform infrared spectrometer (FT-IR)

Infrared spectra were recorded from 400 to 4000 cm$^{-1}$ in transmittance mode by KBr pellet technique.

### Elemental analysis (EA)

The sample and oxygen were combusted at high temperature and the sample was broken down into its elemental components and gas chromatography separated by frontal analysis with quantitative detection by thermal conductivity detector.

### Thermal Gravimetric Analysis (TGA)

TGA is an analytical technique that measures the weight loss (or weight gain) of a material as a function of temperature. The experiment was performed at a temperature range of 24 °C – 800 °C at heating rate of 10 °C/min under nitrogen atmosphere.

### Determination of reductive capacity of Ami-SiO$_2$

Ami-SiO$_2$ (0.07 g) were stirred with 50 mL of D.I. water and pH adjusted to 3 with H$_2$SO$_4$ and titrated with 1 mM KMnO$_4$.

## 3.5 Preparation of gold nanoparticles

Gold nanoparticles were generally prepared by mixing 0.4 g of Ami-SiO$_2$ with 100 mL of 10 mg/L Au(III) solution at pH 3. The mixture was stirred for 30 minutes, and then centrifuged at 3000 rpm for 10 minutes. The resulting solid were separated and dried at approximately 100$^{\circ}$C for 2 hours. The following parameters were investigated to obtain the optimal conditions for the preparation of gold nanoparticles.

### 3.5.1 Effect of pH

The pH of gold solution [AuCl$_4$]$^-$ were studied in the range of 1.0 – 7.0. The basic pH were not studied as gold would be partially converted to Au(OH)$_3$. Gold solution (40 mg/L, 100 mL) was added to Ami-SiO$_2$ (0.4 g) in 150 mL beaker. The mixture was stirred for 30 minutes at room temperature. The mixture was centrifuged at 3000 rpm for 10 minutes. The centrifugate was separated and the amounts of residual Au(III) was determined by FAAS. The particles were filtered with polyethylene frits until dry and stored in a vial for 1 week. After that, the solid was characterized by XRD, DR-UV-Vis, and TEM.

**Characterization of gold nonaparticles**

**X-ray diffractometry (XRD)**

XRD was used for the characterization of crystallite pattern of gold nanoparticles in the range 10-90 two theta.

**Diffuse reflectance ultraviolet-visible spectrophotometry (DR-UV-Vis)**

DR-UV-Vis spectrophotometer was used for absorbance measurements of gold nanoparticles with the wavelength range of 350-800 nm with the reflectance mode.

**Transmission electron microscopy (TEM)**

TEM was performed with a JEM-2001 instrument at 200 kV. Samples for TEM were prepared by placing a drop of the ethanol suspension of the nanopowders onto carbon grids and pre-dried before insertion.

### 3.5.2  Effect of Au(III) concentration

The concentration of gold solution $[AuCl_4]^-$ was varied from 10-200 mg/L at the optimum pH. Gold solution (10 mL) was added to a test tube containing 25 mg of Ami-SiO$_2$. The mixture was stirred for 30 minutes at room temperature. The mixture was centrifuged at 3000 rpm for 10 minutes. The centrifugate was separated and the amounts of residual Au(III) was determined by FAAS.

The concentration of gold solution $[AuCl_4]^-$ was then varied from 10-60 mg/L at the optimum pH. Gold solution (100 mL) was added to Ami-SiO$_2$ (0.4 g) in 150 mL beaker. The mixture was stirred for 30 minutes at room temperature, then centrifuged at 3000 rpm for 10 minutes. The centrifugate was separated and the amounts of residual Au(III) was determined by FAAS. These particles were filtered with polyethylene frits, air dried and kept in vials for 1 week. After that, the solid was characterized by XRF, TEM, XRD and DR-UV-Vis.

### 3.5.3  Effect of nanoparticle formation time

The 40 mg/L gold solution (100 mL) with optimum pH was added to Ami-SiO$_2$ (0.4 g) in 150 mL beakers. The mixtures were stirred for 30, 60, 120 and 180 minutes. These mixtures were afterwards centrifuged at 3000 rpm for 10 minutes. The centrifugate were separated and the amounts of residual Au(III) were determined by

FAAS. The solids were filtered with polyethylene frits, air dried and kept in vials. After that, the solids were characterized by XRD.

The study of curing time was performed by further curing the particles for 1 and 3 days. The particles were subsequently characterized by XRD.

### 3.5.4  Effect of interfering ions

In this section, the influence of four different interfering ions, namely 100 mg/L $Ag^+$, $Cu^{2+}$, $Ni^{2+}$ and $Zn^{2+}$, on the formation of gold nanoparticles were studied. Each of these ions were individually added to the gold solution forming a bi-component mixture. The mixed metal solutions were then added to Ami-SiO$_2$ (0.4 g) in 150 mL beaker. The mixtures were stirred for 30 minutes at room temperature and then centrifuged at 3000 rpm for 10 minutes. The centrifugates were separated and the amounts of residual metals were determined by FAAS. The solids were filtered with polyethylene frits, air dried and kept in vials for 1 week. After that, the solids were characterized by XRF, XRD and TEM.

### 3.5.5  Effect of cyanide ions ($CN^-$)

Au(III) cyanide $[Au(CN)_4]^-$ solution was prepared by adding excess amount of KCN to the Au(III) solution. The pH of the solution were adjusted to pH 3 and 10.5 to imitate acidic and basic wastes respectively. The mixtures were then addded to 0.4 g Ami-SiO$_2$ in 150 mL beaker. These mixtures were stirred for 30 minutes at room temperature then centrifuged at 3000 rpm for 10 minutes. The centrifugates were separated and the amounts of residual Au were determined by FAAS.

## 3.6    Applications of Ami-SiO$_2$

### 3.6.1  Recovery of gold on Ami-SiO$_2$

This experiment aims to evaluate the recovery of gold adsorbed on the functionalized silica. The composite materials (Au-Ami-SiO$_2$) from 3.5.1 and 3.5.2 which were prepared under different pHs and concentrations were mixed with 2 mL of aqua regia to elute the gold contents. The mixtures were then filtered by polyethylene micro filter and the filtrates were adjusted to 10 mL with DI water. These solutions were then analyzed for the amount of Au by FAAS and the recovery percentages were calculated.

### 3.6.2  Preparation of gold nanoparticles from jewelry industry

### wastewater

A sample of jewelry-related wastewater was obtained from the precious metal testing lab of the Gem and Jewelry Institute of Thailand. This solution contains Au(III) at about 120 mg/L and the solution pH is about 0.15. The solution was filtered by 0.45 µm membrane filter, then adjusted to the optimum pH. This solution was then mixed with 0.4 g of Ami-SiO$_2$ in a 150 mL beaker. The mixture was stirred for 30 minutes at room temperature and centrifuged at 3000 rpm for 10 minutes. The centrifugate was separated and the amount of residual Au(III) was determined by FAAS. The particles were filtered with polyethylene frits, air dried and kept in vial for 1 week. After that, the particles were characterized by XRF, XRD and TEM.

After the characterization was completed, the impurities on gold nanoparticles were eluted with 1M HCl (20 mL), 1M HNO$_3$ (20 mL), 1M HNO$_3$ (40 mL) + H$_2$O$_2$ (10 mL) and 1M KOH (40 mL) + H$_2$O$_2$ (10 mL). The mixtures were filtered by polyethylene micro filter. The residual Au(III) was determined by FAAS and the particles were again characterized by XRF, XRD and TEM.

# CHAPTER IV

# RESULTS AND DISCUSSION

## 4.1 Characterization of amido-amidoxime functionalized silica

The functionalized silica was characterized by ^{13}C-NMR solid state, elemental analysis, FT-IR spectroscopy and TGA. The results of which are shown below.

### 4.1.1 Carbon nuclear magnetic resonance spectrometry (^{13}C-NMR)
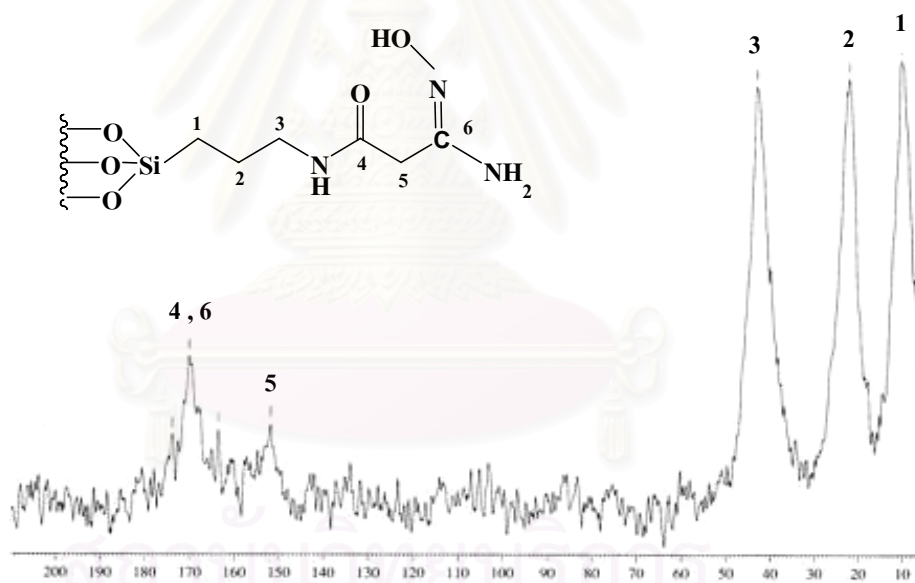


**Figure 4.1** ^{13}C-NMR spectrum of Ami-SiO$_2$.

The ^{13}C-NMR spectrum (Figure 4.1) revealed peaks at approximately 10, 21 and 42 ppm which corresponded to the three alkyl chain carbons, Si-**C**H$_2$, CH$_2$-**C**H$_2$-CH$_2$ and **C**H$_2$-NH, respectively. The higher field peak around 170 ppm could be attributed to the carbons of the amide (**C**O-NH) and the oxime (**C**=N-OH) groups. The remaining carbon, adjacent to carbonyl carbon (CO-**C**H$_2$), was found at 151 ppm. This result clearly indicated a successful synthesis of Ami-SiO$_2$.

### 4.1.2 Fourier transform infrared spectroscopy (FT-IR)

The FT-IR spectrum of the original silica and functionalized silica are illustrated in Figure 4.2. The characteristic peaks of silica at around 1100 cm$^{-1}$ due to Si-O stretching along with 786 and 450 cm$^{-1}$ which correspond to Si-O-Si stretching were shown in all cases.

The FT-IR spectrum of the functionalized silica obtained from each synthesis step (i.e. AP-SiO$_2$, CA-SiO$_2$ and Ami-SiO$_2$) revealed a transformation from AP-SiO$_2$ (C-H stretching at 2953 cm$^{-1}$ and N-H bending at 1600 cm$^{-1}$) to CA-SiO$_2$ (C-N stretching 1343 cm$^{-1}$ and C≡N stretching at 2248 cm$^{-1}$) and finally to Ami-SiO$_2$ (C=N stretching at 1628 cm$^{-1}$). These results further confirmed the successful synthesis of the proposed functionalized silica.
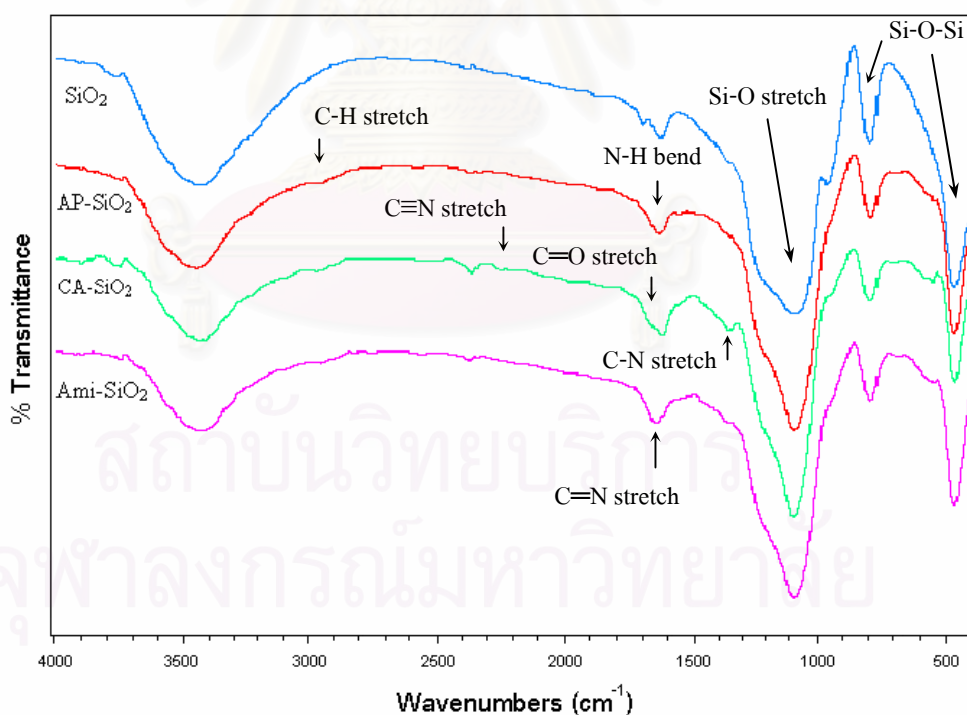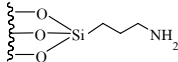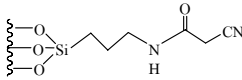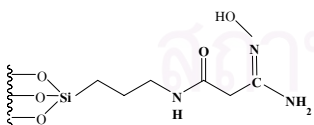
**Figure 4.2** FT-IR spectra of SiO$_2$, AP-SiO$_2$, CA-SiO$_2$ and Ami-SiO$_2$ in KBr.

### 4.1.3 Elemental analysis (EA)

The elemental analysis was carried out after each step of the synthesis pathway as reported in Table 4.1.

**Table 4.1** Elemental composition and atomic ratios of the functionalized silica

| Sample | | %C | %H | %N | C/N ratio |
|---|---|---|---|---|---|
| $SiO_2$ | exp | 0.05 | 0.01 | 0.06 | 0.972 |
| | cal | - | - | - | - |
| AP-$SiO_2$ | exp | 5.89 | 0.98 | 2.35 | 2.974 |
| | cal | 26.85 | 6.01 | 10.44 | 3.000 |
| Cf : $C_3H_8NO_3Si$ | | | | | |
| CA-$SiO_2$ | exp | 9.07 | 1.06 | 3.85 | 2.775 |
| | cal | 35.81 | 4.51 | 13.92 | 2.999 |
| Cf: $C_6H_9N_2O_4Si$ | | | | | |
| Ami-$SiO_2$ | exp | 5.97 | 1.57 | 2.76 | 2.557 |
| | cal | 30.76 | 5.16 | 17.94 | 1.999 |
| Cf: $C_6H_{12}N_3O_5Si$ | | | | | |

Cf = chemical formula, exp = experimental value, cal = calculated value.

The elemental analysis was used to monitor changes in the percentages of C, H and N of the organic moieties following each step of the synthesis. The theoretical

values were also presented for comparison. It was clearly seen that the calculated values are significantly larger than the experimental values mainly because they were calculated based on the assumption that all of the silica are occupied by the organic functionalities. In reality, only an undetermined and probably small portion of the phase were reacted and thus resulted in much smaller values for these elements. In order to overcome the questionable contribution of the silica phase, the C/N ratio was used to compare the two values as this ratio would not be affected by the loading amount of organic moieties on the phase. The C/N ratios of both experimental and calculated value of AP-SiO$_2$ are almost identical suggesting that the conversion of the phase in this initial step was complete. These ratios were slightly different in the following steps. As the reaction proceeded, C/N ratio would theoretically become smaller due to the addition of amide and oxime groups respectively. However, the experimental values were slightly larger than expected, presumably because the conversion of functionalities might not be complete.

### 4.1.4   Thermal gravimetric analysis (TGA)

The thermogravimetric (TGA) and derivative thermogravimetric (DTG) curves of silica and functionalized silica were shown in Figure 4.3. The experiment was conducted with a heating rate of 10 $^{o}$C/min. Only one peak at 80-150$^{o}$C was observed for pure silica, most likely due to the loss of water physically adsorbed on the phase. On the other hand, a continual loss of weight was observed in the range of 200-600$^{o}$C for all of the functionalized silicas. These changes were probably due to the decomposition of organic moieties on the sorbent in each step. However, TGA was unable to provide sufficient evidence as to which functionality was incorporated into the silica.
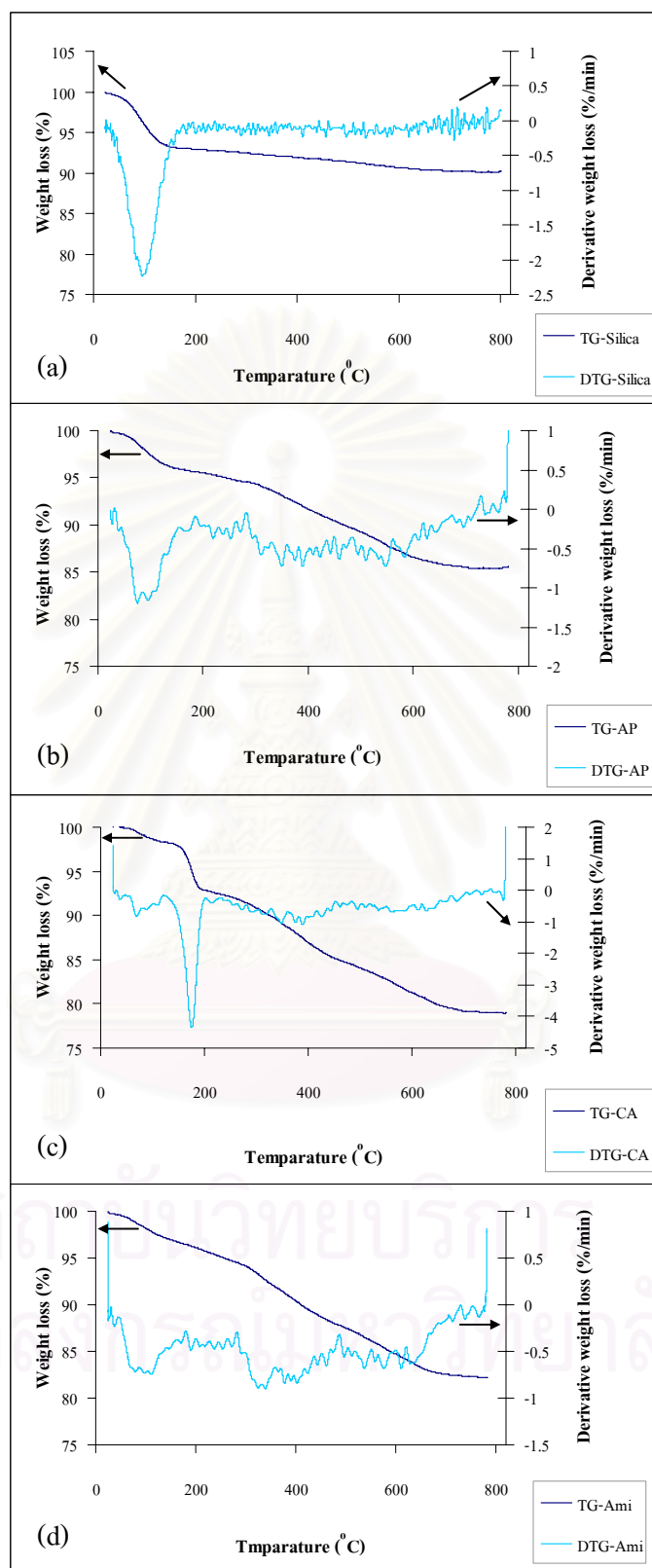
**Figure 4.3** Thermogravimetric and derivative thermogravimetric curves of (a) silica, (b) AP-SiO$_2$, (c) CA-SiO$_2$ and (d) Ami-SiO$_2$.

### 4.1.5 Determination of reductive capacity of Ami-SiO$_2$

Based on the proposed mechanism of the synthesis, the final product of functionalized silica (Ami-SiO$_2$) contains an oxime (**C**=N-OH) group which is a potentially reductive functionality. Therefore, the determination of reductive ability of the modified silica can be used to further confirm the successful conversion of the phase. Moreover, the reductive capacity of the Ami-SiO$_2$ would also provide an insight into how much silica are actually functionalized.

The reduction ability of the synthesized silica was determined by titration with KMnO$_4$. The purple color of KMnO$_4$ solution became colorless as the reaction with Ami-SiO$_2$ proceeded toward the end point indicating a definite reduction by the phase. The end point was observed by the precipitation of MnO$_2$ according to the equations (4.1.1) and (4.1.2) [48].

$$MnO_4^-(aq) + 8H_3O^+(aq) + 5e^- \rightleftharpoons Mn^{2+}(aq) + 12H_2O \qquad (4.1.1)$$

$$2MnO_4^-(aq) + 3Mn^{2+}(aq) + 6H_2O \rightleftharpoons 5MnO_2(s) + 4H_3O^+ \qquad (4.1.2)$$
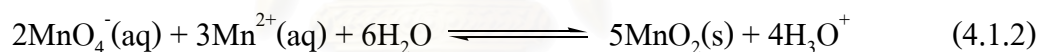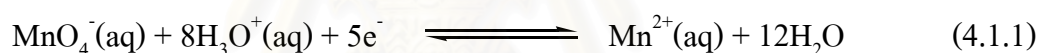
Since the definite formula and loading of the functional group onto silica was not known, the reduction capacity of Ami-SiO$_2$ was alternatively derived as the equivalent (E$_q$) of KMnO$_4$ by the following equations [49].

$$EqW = \frac{M.W.}{e^- \text{ change}} \qquad (4.1.3)$$

$$Eq = \frac{weight (g)}{EqW} \qquad (4.1.4)$$

EqW = Equivalent weight

Eq = Equivalent

M.W. = molecular weight

The reductive capacity was found to be 1.6±0.1 mEq/g Ami-SiO$_2$. Moreover, the original silica, AP-SiO$_2$ and CA-SiO$_2$ were also evaluated and no such reducing properties were found, thus validating the proposed synthesis pathway of the reducing sorbent Ami-SiO$_2$.

## 4.2 The preparation of gold nanoparticles

Gold (Au(III)) was the subject of this study under the postulation that it can be reduced and supported as nanoparticles by the functionalized sorbent. The reaction was conducted by simply mixing the chloroaurate (AuCl$_4^-$) solution with the functionalized sorbent (Ami-SiO$_2$), then left stirring for a certain period and the composite materials (Au-Ami-SiO$_2$) was recovered. Various parameters that may have influences on the formation of these gold nanoparticles were evaluated as detailed below.

### 4.2.1 Effect of pH

The effect of pH (1-7) of the Au(III) solution on the formation of gold nanoparticles were evaluated. The basic pHs were not studied as this may result in the destruction of silica based structure. Moreover, it has been previously reported that gold can form a hydroxide complex, [AuCl$_3$(OH)]$^-$, starting from pH 7.2 [50] and the replacement of chloride by hydroxide ions in the coordination sphere of [AuCl$_4$]$^-$ would also result in the change of reduction potential of Au(III) [15].

In this experiment, the residual concentrations of gold in the solution were analysed to determine the gold contents adsorbed on the functionalized silica. The adsorption capacity of gold on the sorbent was displayed as a function of pH in Figure 4.4. Highly acidic medium (pH 1) resulted in the least amount of gold adsorbed on the phase. This is probably due to the majority of the active sites on the functionalized silica being destroyed and thus becoming inactive. The adsorption capacity increases

with pH and reaches a maximum plateau (no residual Au detected) at around pH 3 with a capacity of approximately 10 mg Au/g Ami-SiO$_2$.
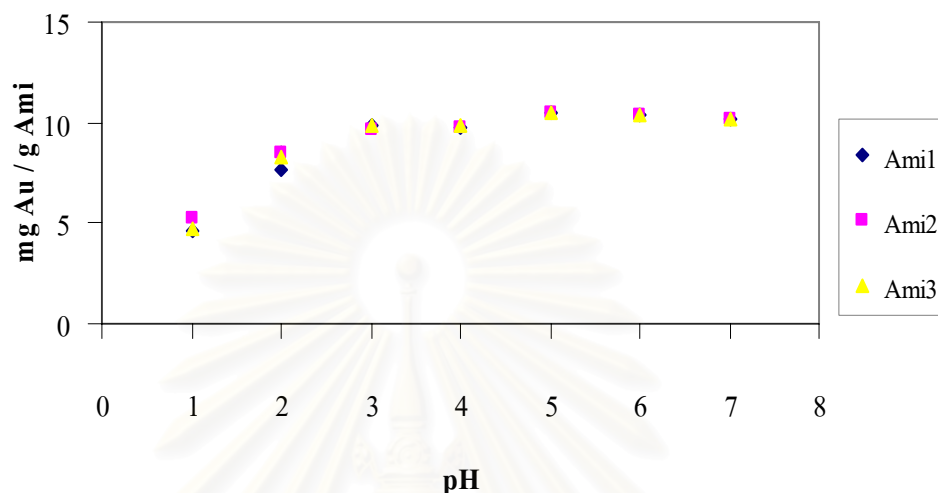


**Figure 4.4** Effect of pH on the adsorption capacity.

Nonetheless, the capacity only demonstrated the amount of gold adsorbed on the phase but did not indicate which form they were in. Figure 4.5 exemplified the composite materials obtained from the reaction under varying pH. The characteristic purple color of gold nanoparticles were clearly observed at pH 3 and slightly less so for pH 2, 4 and 5. Virtually no color changes were seen for pH 1, 6 and 7.



**Figure 4.5** Composite materials obtained from the reaction under different pH.

This observation is an early indication that the reduction of Au(III) by the amidoxime group into the gold nanoparticles can be achieved and optimized at pH 3 and slightly less in the adjacent pHs. A very high acid content (pH 1) would lead to the unstability of the amidoxime group and so the reduction would not be expected. As the

reaction moved to the other end (pH 6-7), the amide bond in Ami-SiO$_2$ might be hydrolysed and thus resulted in the loss of reductive property.

These visual findings were confirmed by the characterization of the sorbent utilizing X-ray diffraction (XRD), diffuse reflectance ultraviolet-visible spectrophotometry (DR-UV-Vis) and transmission electron microscopy (TEM) techniques.
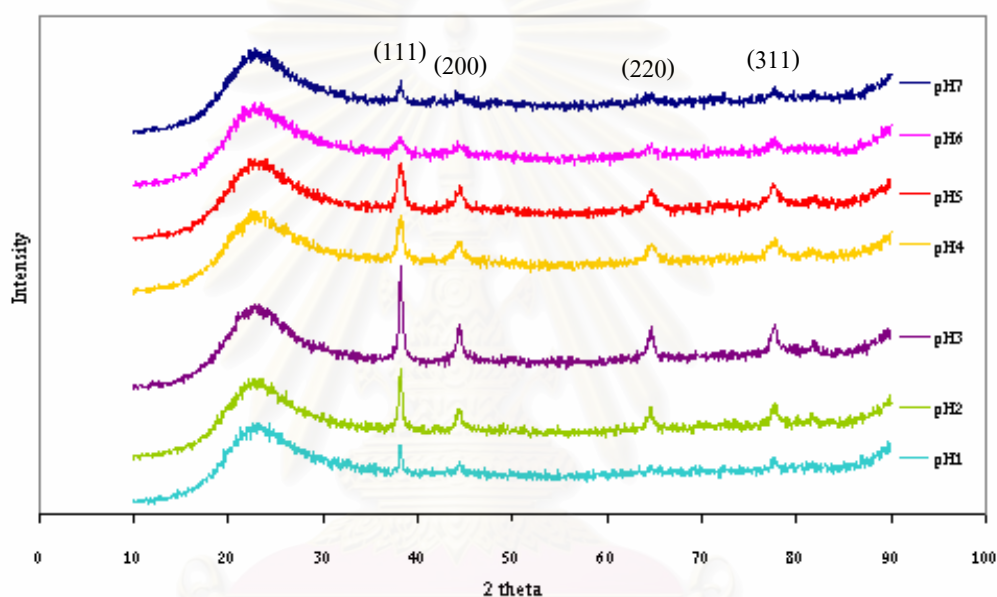


**Figure 4.6** XRD patterns of gold nanoparticles on Ami-SiO$_2$ at different pH.

The XRD patterns in Figure 4.6 illustrated the composition of gold crystallites at different pH. The peaks located at 36, 44, 64, and 78$^{\circ}$ two theta correspond to the 111, 200, 220, and 311 planes of a faced centered cubic lattice of gold respectively [51]. The broad peak that appeared around 17$^{\circ}$-30$^{\circ}$ was due to the amorphous silica characteristic. By applying the scherrer equation on the most intense peak of (111) reflection, the gold crystalline sizes were determined to be in the range of 14.1-23.8 nanometers. Au-Ami-SiO$_2$ at pH 3 showed the highest (111) peak area and its crystalline size of 21.2 nm was among the larger ones.

The DR-UV-Vis absorption spectra of the sorbents were shown in Figure 4.7. The surface plasmon band of gold nanoparticles were typically characterized at around 520-570 nm and the shift to higher wavelength normally suggests the agglomeration and the increase of the particle size [52]. As could be seen from the figure, the spectra of the sorbents obtained with pH 2 -5 exhibits the nanogold surface plasmon band at approximately 540 nm. The sharpest band of Au-Ami-SiO$_2$ at pH 3 indicated a more uniform size of gold particles.
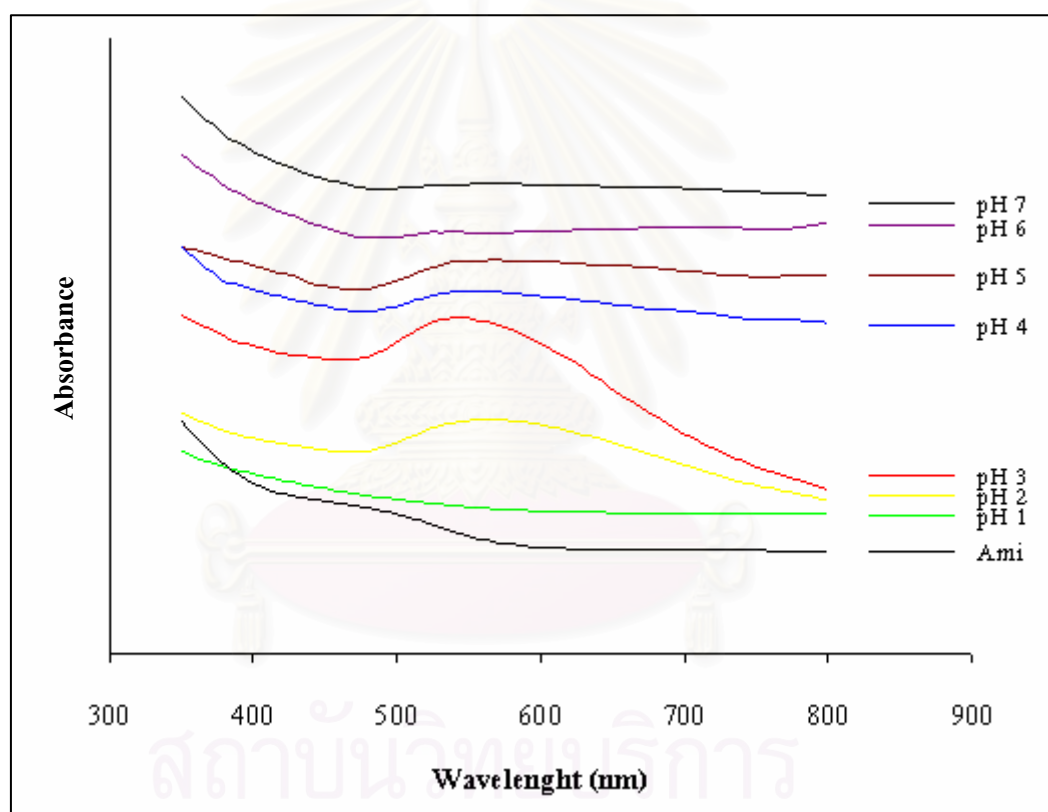


**Figure 4.7** DR-UV-Vis absorption spectra of Ami-SiO$_2$ (Ami) and Au-Ami-SiO$_2$ at different pH.

The presence of gold nanoparticles and its size on the sorbent at different pH were confirmed by TEM micrographs in Figure 4.8 Comparing to the light color of Ami-SiO$_2$ amorphous phase, the dark cubic crystals of nanogold were clearly

presented on the phase at pH 2-7 bearing the sizes within the approximate range of 10-80 nm. The average particle size was calculated by formula (2.4.3).
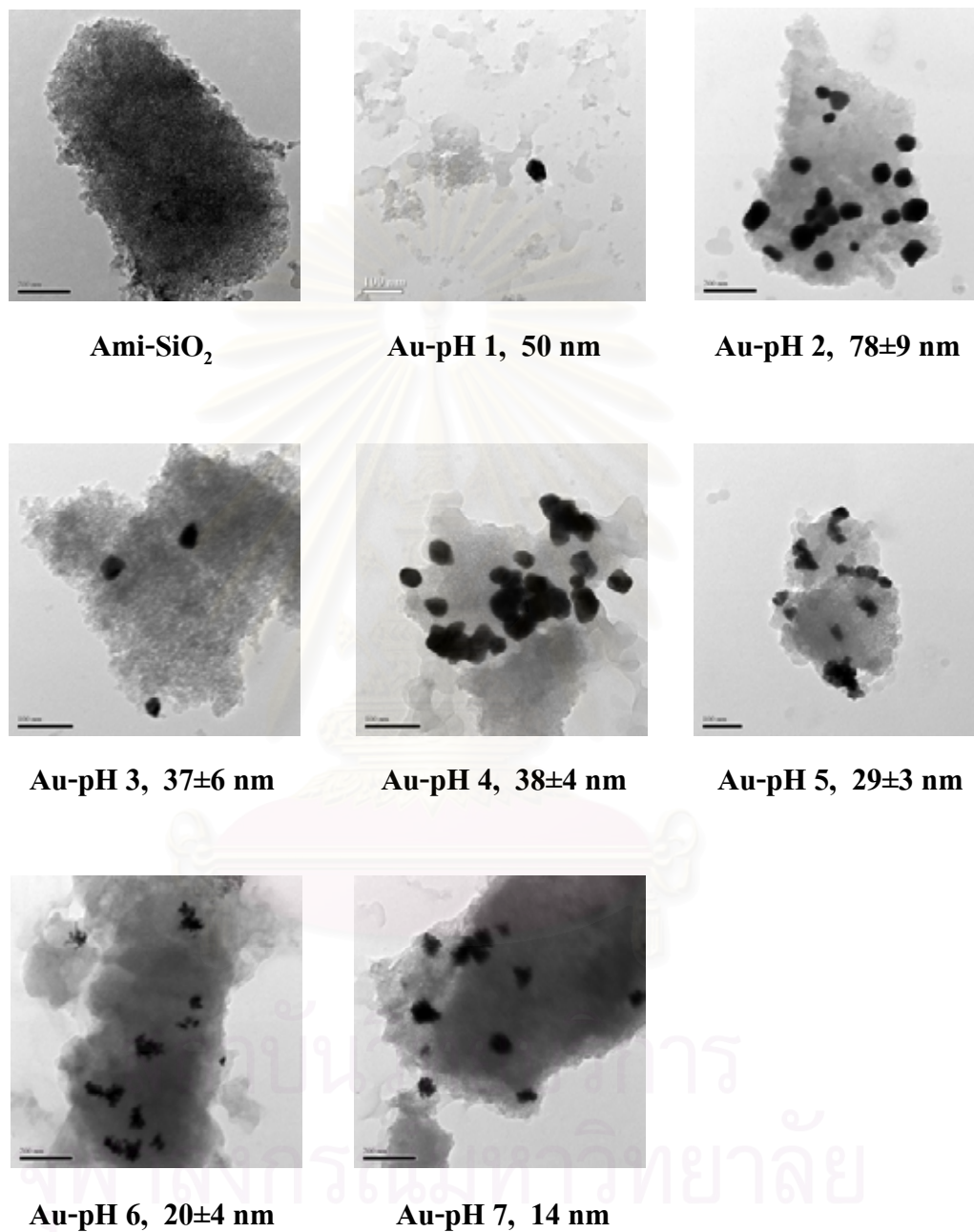


**Figure 4.8** TEM micrographs of Ami-SiO$_2$ and gold nanoparticles at different pH.

Based on all of the previous results, it would be concluded that the formation of gold nanoparticles on Ami-SiO$_2$ was optimized at pH 3 and thus this condition was used for the subsequent experiments.

### 4.2.2  Effect of Au(III) concentration

The effect of Au(III) concentration on the adsorption capacity of Ami-SiO$_2$ was investigated by reacting Au(III) of various concentrations with the sorbent and the remaining amount of Au(III) in the solution was determined by FAAS.
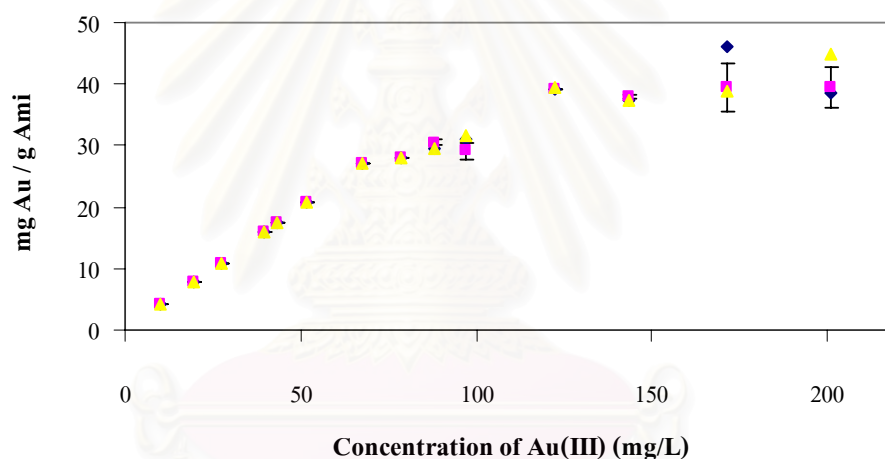


**Figure 4.9**  Effect of concentration of Au(III).

Figure 4.9 demonstrated the adsorption capacity of Ami-SiO$_2$ towards Au(III) of varying concentrations. It was seen that the adsorption capacity of the phase increased proportionally with the concentration of Au(III) up to around 70 mg/L and rose more slowly afterwards to reach a plateau at around 120 mg/L. The maximum capacity of 39±0.1 mg Au/g Ami-SiO$_2$ was observed with 170 mg/L Au solution. This value corresponded to approximately 0.63 mEq / g Ami-SiO$_2$, less than half of the reductive capacity of the sorbent. These results suggested that there was a certain limit in the amount of gold that can be adsorbed on the phase regardless of its concentration.

In order to seek for an insight into what really happened when the gold were adsorbed on the phase, Au-Ami-SiO$_2$ were prepared with Au(III) solution of various concentrations in the range of 10-70 mg/L. The actual concentrations of gold in the solution were determined by FAAS. Higher concentrations were not used because the maximum capacity was already attained from previous observations. The composite particles obtained were then characterized by XRF, TEM, XRD, and DR-UV-Vis respectively.
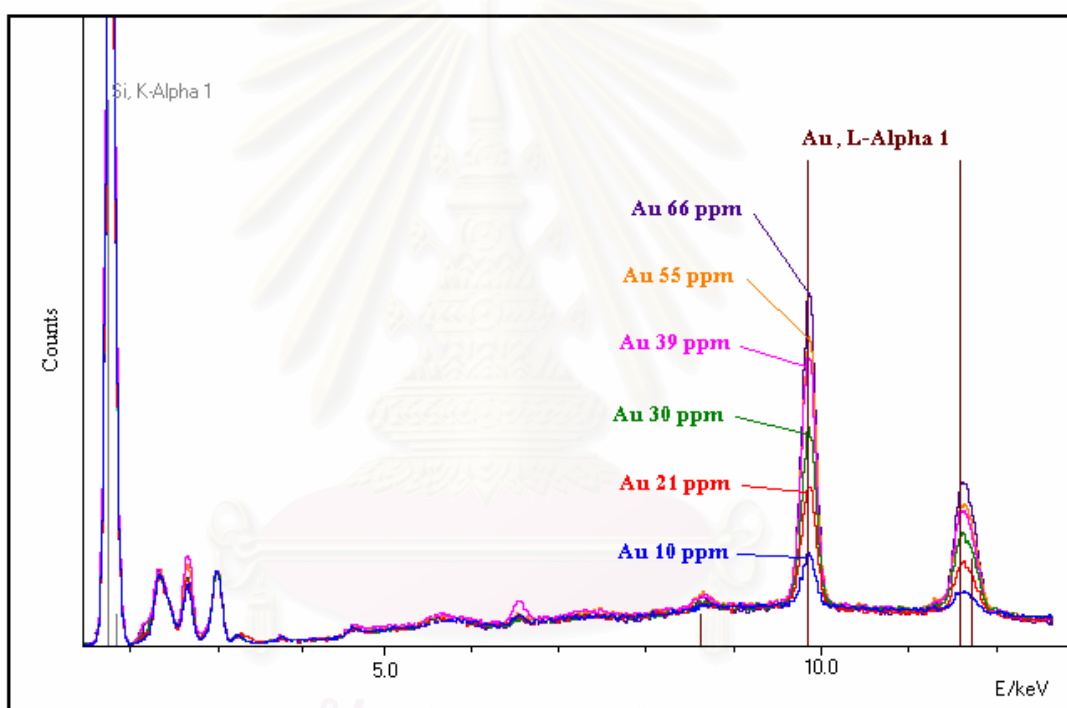


**Figure 4.10** XRF spectra of gold on Ami-SiO$_2$ at different Au(III) concentrations.

Figure 4.10 illustrated the presence of gold on the sorbent. The gold contents in the samples increased as the initial concentration of the gold solution becomes larger. This observation reiterated the result in the previous section that, within the selected initial concentrations, virtually all of the gold can be adsorbed on the Ami-SiO$_2$.

The TEM micrographs (Figure 4.11) show that there were gold nanoparticles present on the sorbent with the size in the range of 20-50 nm. In addition, the size of

these nanogold particles seem to grow as a function of the Au concentration, yet the maximum gold crystals of 49±8 nm were achieved when 31 mg/L of Au(III) was used.



| | | |
|---|---|---|
| **Au 10 mg/L, 27±1 nm** | **Au 21 mg/L, 25±5 nm** | **Au 31 mg/L, 49±8 nm** |
| **Au 40 mg/L, 37±6 nm** | **Au 55 mg/L, 45±8 nm** | **Au 66 mg/L, 45±10 nm** |
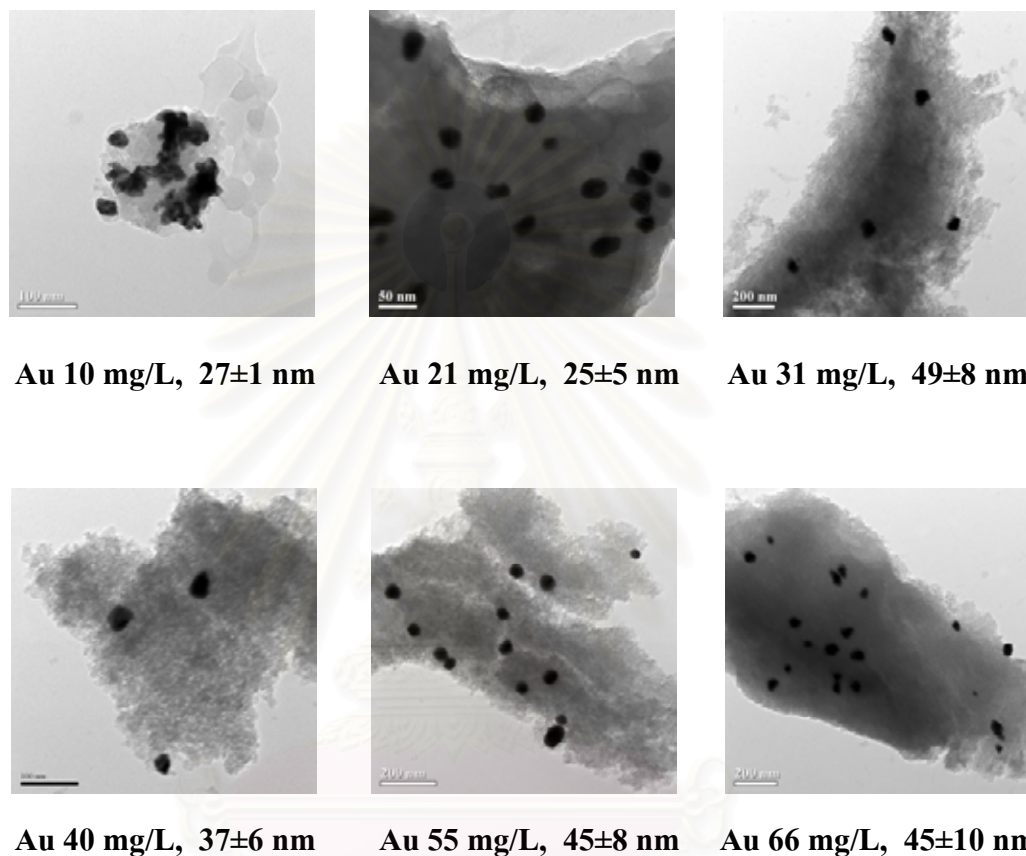
**Figure 4.11** TEM micrographs of gold nanoparticles obtained with different initial concentrations.

However, the XRD and DR-UV-Vis analysis of these materials present a different aspect. The XRD patterns and DR-UV-Vis spectra of Au-Ami-SiO$_2$ obtained from different Au(III) concentrations are displayed in Figure 4.12 and 4.13 respectively.
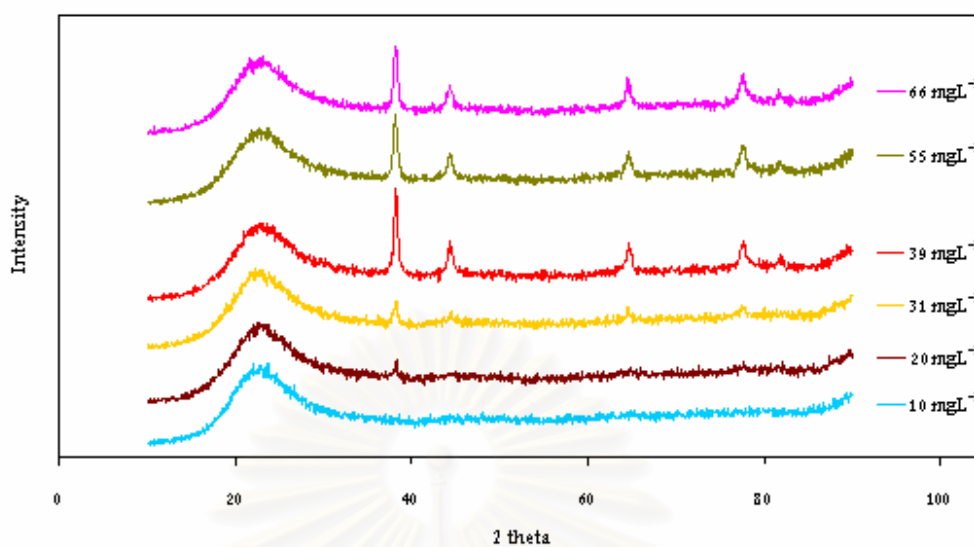
**Figure 4.12** XRD patterns of gold nanoparticles on Ami-SiO$_2$ at different

initial concentrations.
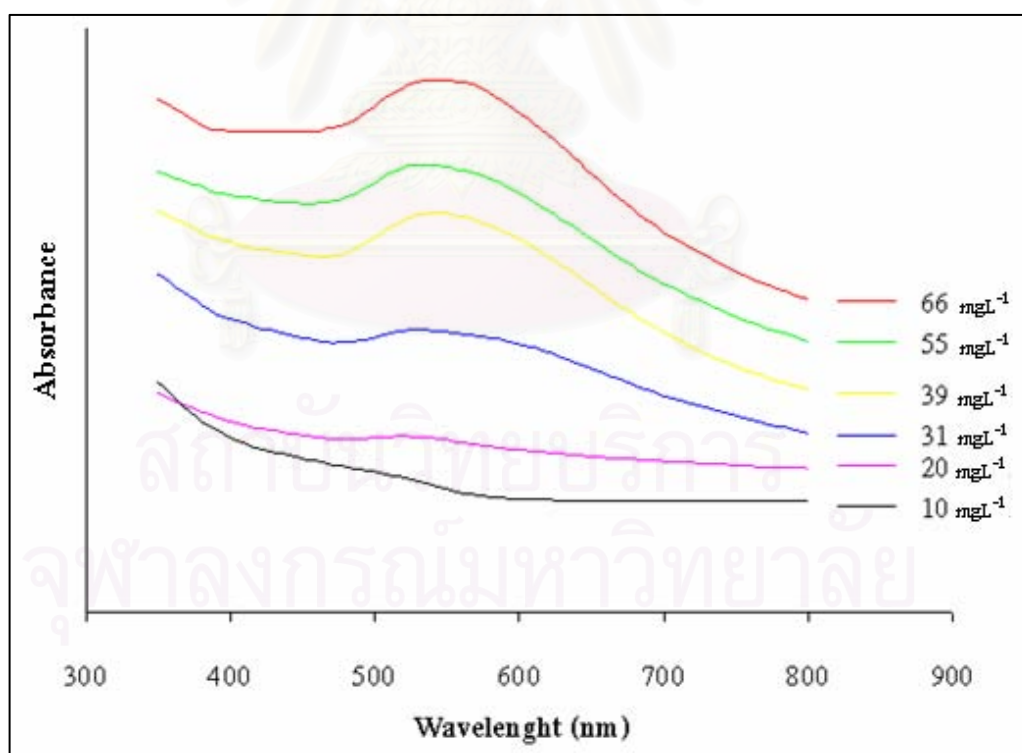


**Figure 4.13** DR-UV-Vis absorption spectra of gold nanoparticles on Ami-SiO$_2$ at

different initial concentrations.

The Au-Ami-SiO$_2$ showed clearly a characteristic XRD pattern of gold nanoparticle and the highest (111) peak area at 38$^o$ two theta. The peak areas tended to increase as a function of initial gold concentration and became nearly constant above 39 mg/L. A similar trend was observed for the surface plasmon band of gold nanoparticles (520-570 nm) in the DR-UV-Vis spectra. These results suggest that there was a certain capacity for the formation of gold nanoparticles on the sorbent at approximately 40 mg/L of Au while the XRF indicated that the remaining gold contents can still be adsorbed on the sorbent but probably not as nanogold. Therefore, it can be implied that Au(III) can either be reduced to Au(0) nanoparticles (gold nanoparticles) by the Ami-SiO$_2$ according to equation (4.2.1) [53] and stabilized by the remaining amine functionalities on the surfaces or it can be adsorbed by a different mechanism. The latter case is most likely due to the complexation of gold according to equation (4.2.2) [6].

$$\text{(4.2.1)}$$

$$\text{(4.2.2)}$$
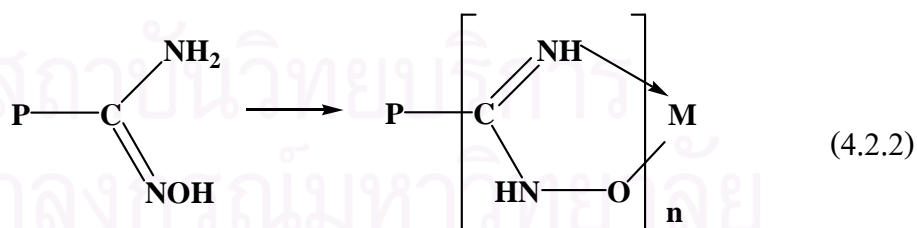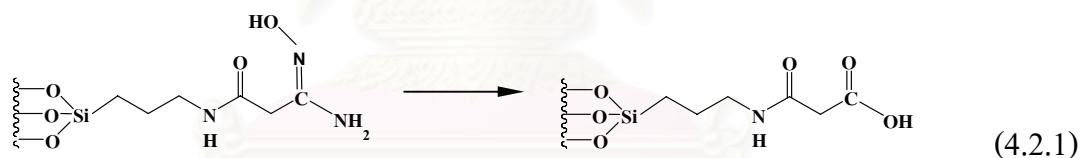
### 4.2.3 Effect of nanoparticle formation time

In this experiment, the effect of contact time was investigated. The functionalized silicas (Ami-SiO$_2$) were left stirring in the 40 mg/L Au solution for 30, 60, 120 and 180 minutes. The gold nanoparticles were separated afterward, dried and immediately characterized by XRD technique. The result was shown in Figure 4.14.
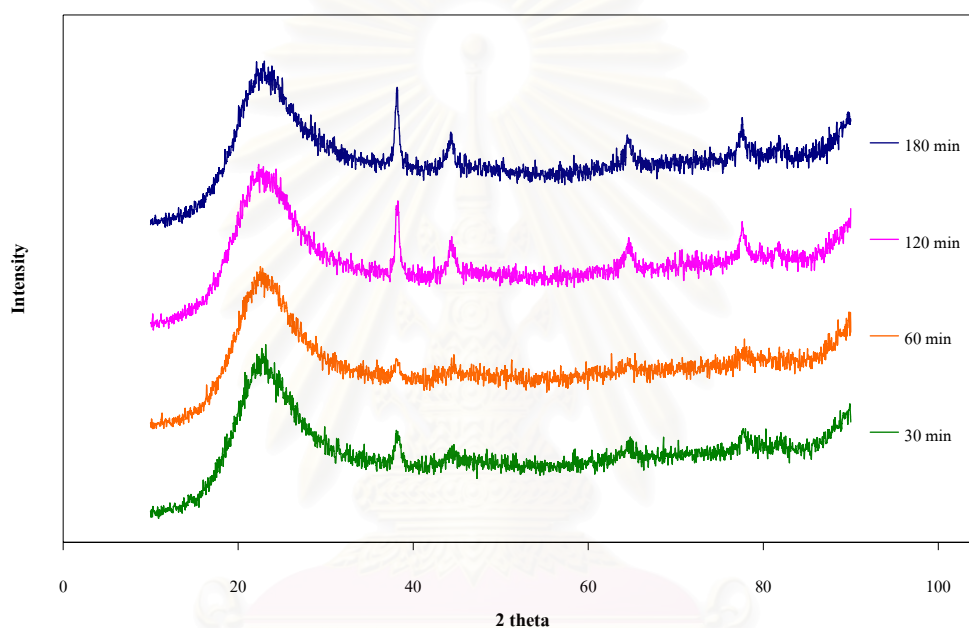


**Figure 4.14** XRD patterns of Au-Ami-SiO$_2$ obtained with different contact time.

After the removal of the sorbent, all remaining solution were analyzed by FAAS and no gold was found indicating that all gold were adsorbed on the surface. As can be seen from the Figure 4.14, longer stirring time resulted in higher amount of gold nanoparticles formed on the sorbent. However, it was also observed that the materials obtained with shorter contact time (30 and 60 min) slowly changed to purple color when left standing overnight. Presumably, the gold initially adsorbed on the phase could be slowly reduced and became gold nanoparticles upon curing.

The effect of curing time was therefore investigated. The Au-Ami-SiO$_2$ from the previous experiment were cured for 1 day and 3 days prior to the analysis with XRD.
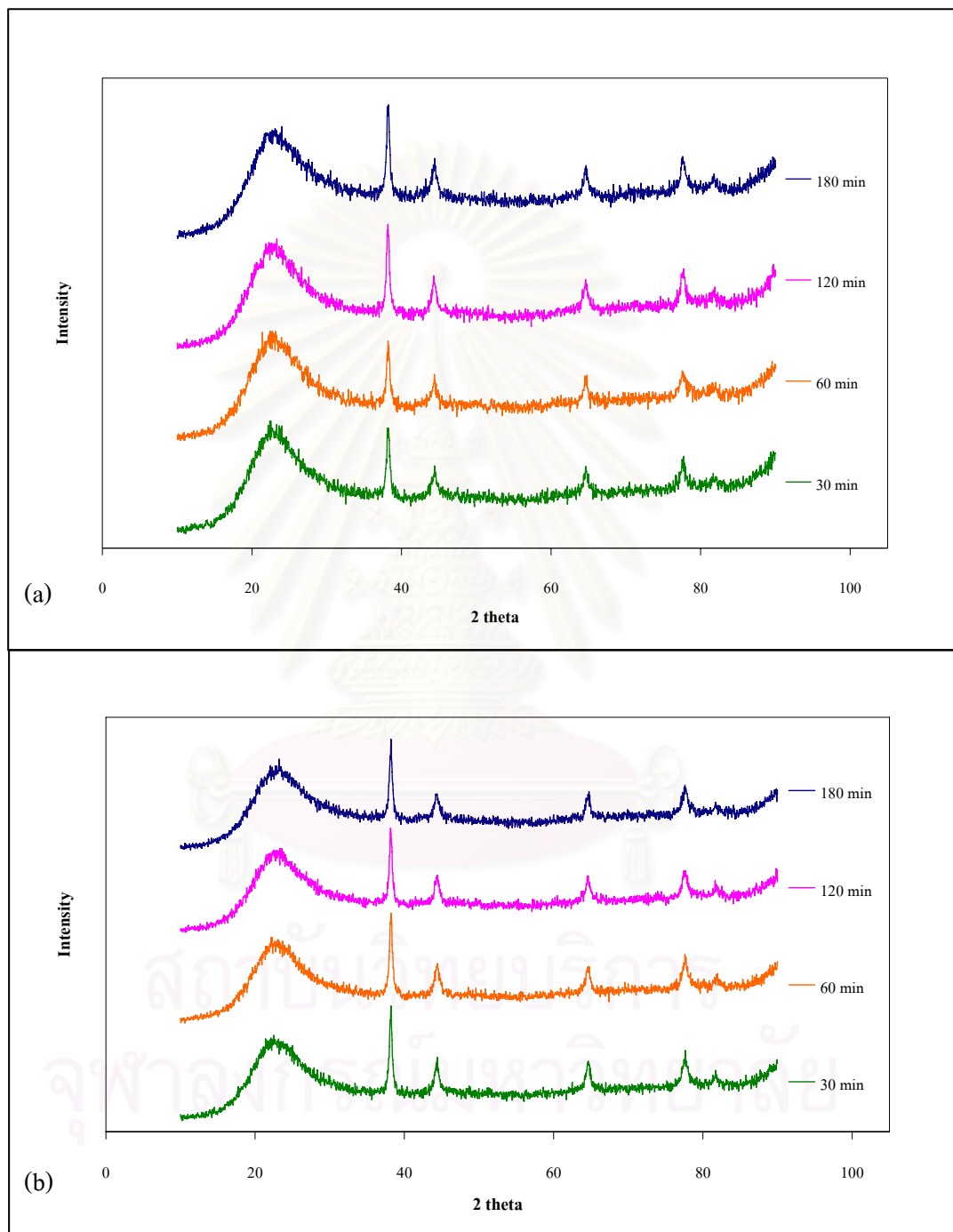


**Figure 4.15** XRD patterns of gold nanoparticles on Ami-SiO$_2$ after the curing time

(a) 1 day  and (b) 3 days.

After 1 day of curing time (Figure 4.15 (a)), a significant increase in the intensity of nanogold peak were observed for all contact times. The addition of nanogold formation were more pronounced for shorter contact times (30 and 60 min). No changes were observed for the longer contact times (120 and 180 min) after 3 days of curing (Figure 4.15 (b)) suggesting that the transformation might have already been completed. The intensities of 30 and 60 min contact time samples were almost identical to those of longer contact times after 3 days of curing and so the conversion into nanogold were presumed complete as well. It can therefore be concluded that both contact time and curing time play an important role in the formation of gold nanoparticles reaffirming the mechanism that the gold might be initially adsorbed and subsequently reduced into Au(0) nanoparticles (gold nanoparticles) which aggregate to larger crystallite sizes (stronger peak) over the period of time.

### 4.2.4   Effect of interfering ions

The potential interference of four different ions commonly found in gold alloys and gold-related applications were investigated in this study. The tested solutions contained 40 mg/L Au and 100 mg/L each of $Ag^+$, $Cu^{2+}$, $Ni^{2+}$, and $Zn^{2+}$, respectively. The concentrations of these interfering ions were initially measured by FAAS. After that, the bi-component mixtures were treated with Ami-$SiO_2$ as discussed previously. After the removal of the sorbent, the remaining amounts of interfering ions in the supernatant were determined once again. The initial and residual concentrations of these ions were presented in Figure 4.16.
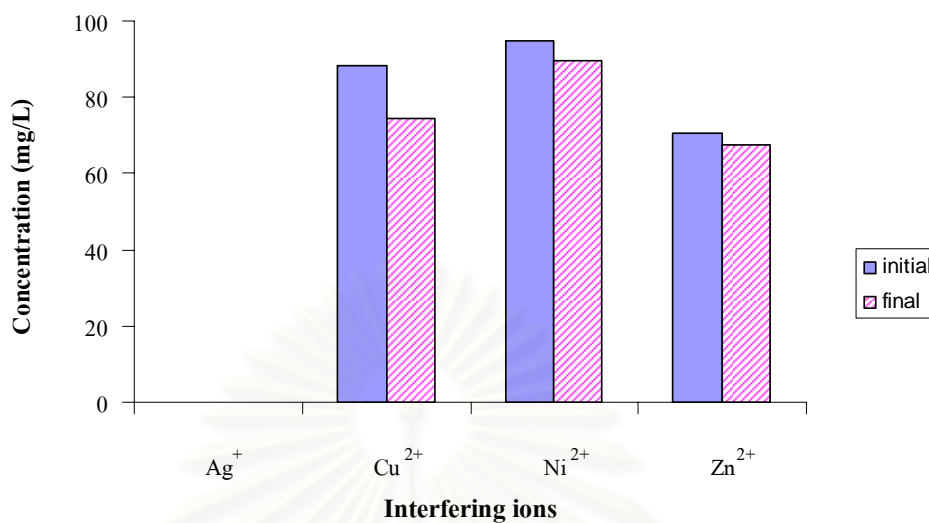
**Figure 4.16** Effect of interfering ions.

In all instances, gold was not found in the solution suggesting a complete adsorption on the phase. It was noticed that silver ions were not present in the solution both before and after the treatment most likely because $Ag^+$ precipitated as AgCl in the acidic solution. Only a slight reduction of concentrations were observed for the remaining three ions after the extraction. The loss of these ions could be attributed to the complexation with amidoxime functional group on the functionalized silica [54, 55]. Unlike gold, the reduction of these interfering ions were not expected as their reduction potentials ($E^o$) were far lower than that of $Au^{3+}$ (Table 4.2) [56].

**Table 4.2**  Reduction potential of selected metal ions

| Half-reaction | Reduction potential ($E^o$) |
|---|---|
| $Au^{3+}$ + $3e^-$ = Au | 1.52 |
| $Ag^+$ + $e^-$ = Ag | 0.7991 |
| $Cu^{2+}$ + $2e^-$ = Cu | 0.340 |
| $Ni^{2+}$ + $2e^-$ = Ni | -0.257 |
| $Zn^{2+}$ + $2e^-$ = Zn | -0.7626 |

The adsorption of interfering ions on the sorbent were verified by XRF. The XRF patterns (Figure 4.17) clearly illustrated that interfering ions were adsorbed on the phase.

The occurrence of gold nanoparticles were also confirmed by XRD and TEM. The XRD patterns in Figure 4.18 all showed characteristic peaks of the original gold nanoparticles similar to those observed earlier. The size of the gold particles as determined by TEM (Figure 4.19) were in the range of 30-60 nm. These results suggested that the formation of nanogold were not affected by any of the interfering ions.
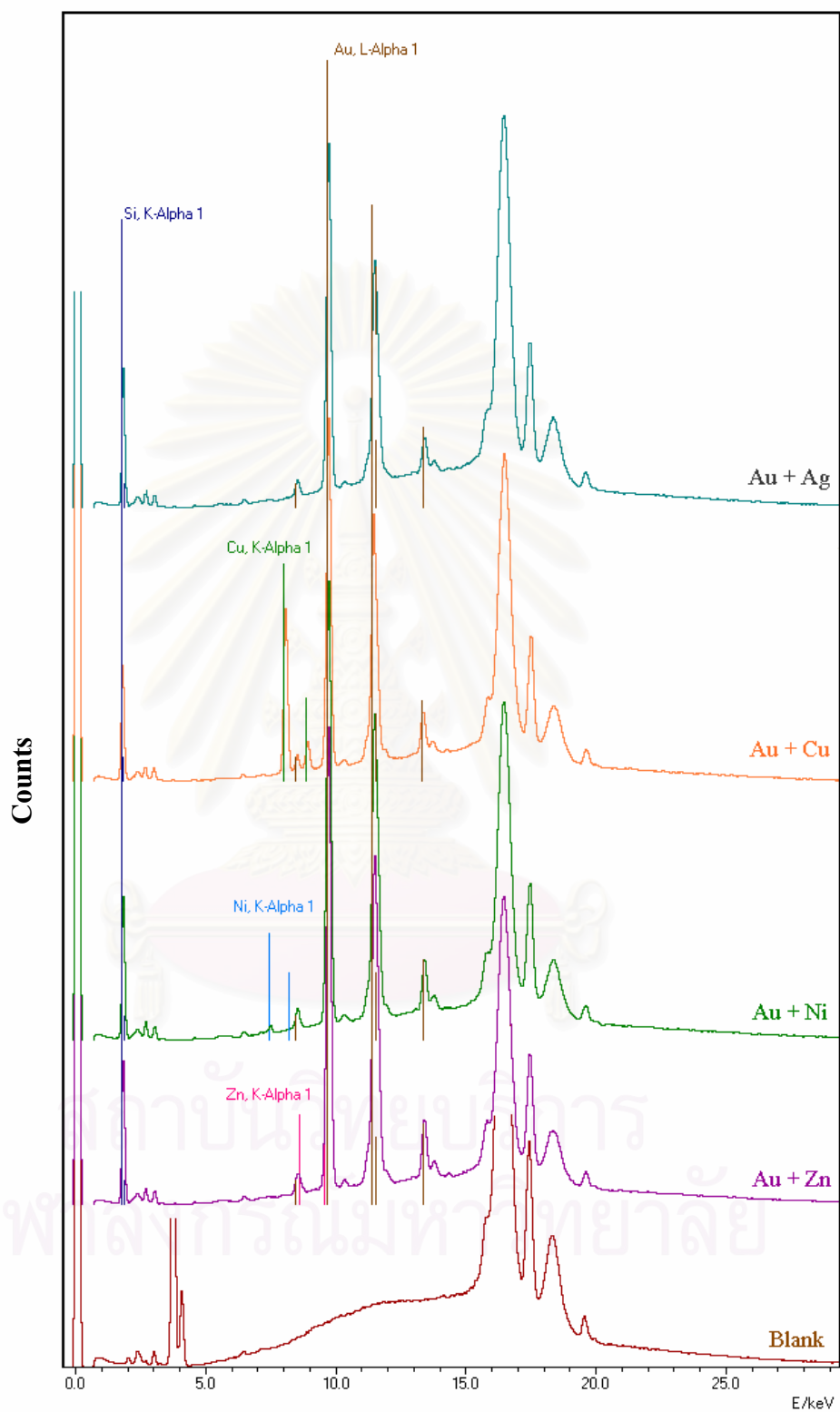
**Figure 4.17**  XRF patterns of gold nanoparticles and interfering ions on Ami-SiO$_2$.
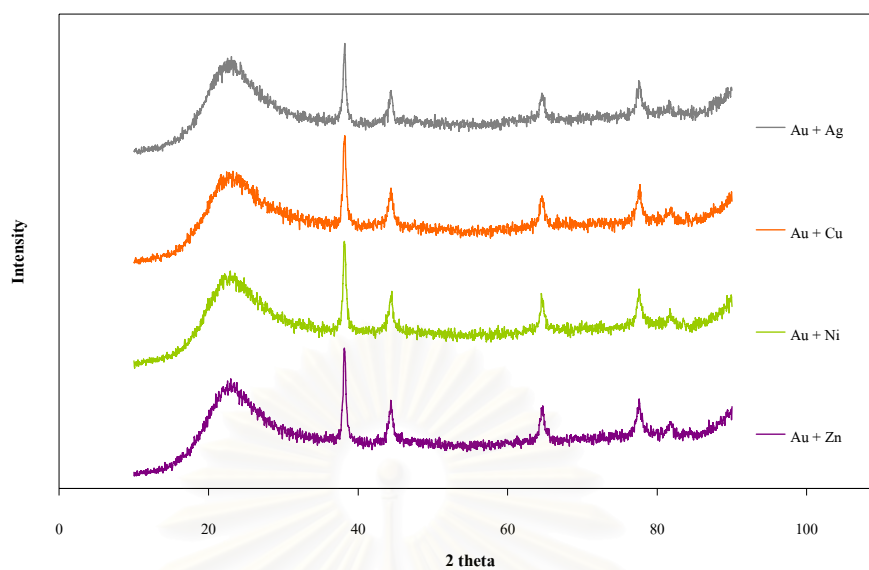
**Figure 4.18** XRD patterns of gold nanoparticles and interfering ions on Ami-SiO$_2$.



Au+Ag, 33±5.7 nm          Au+Cu, 50±11.1 nm

Au+Ni, 55±9.7 nm          Au+Zn, 57±7.5 nm
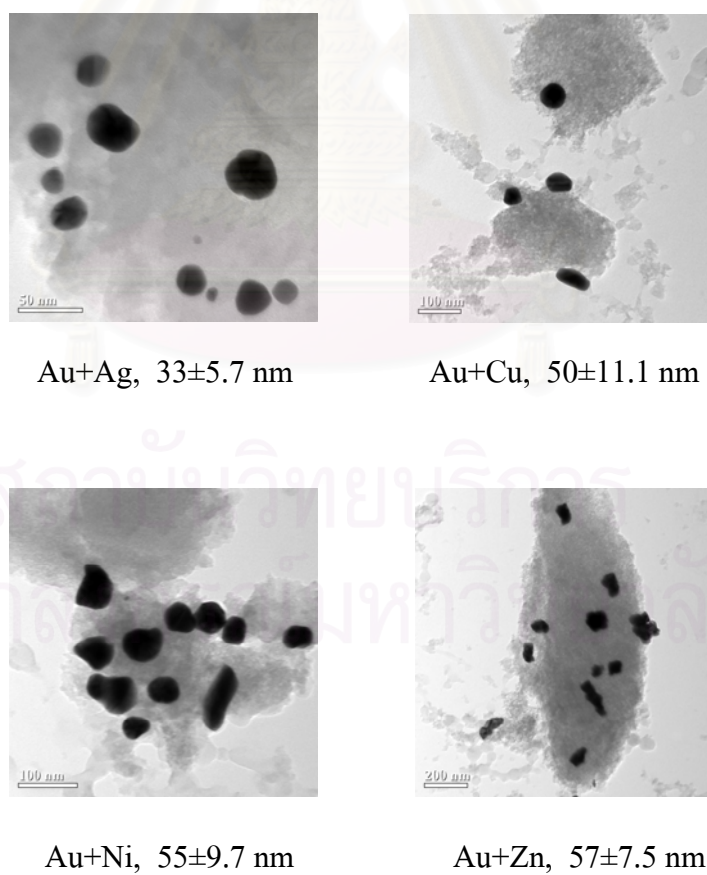
**Figure 4.19** TEM micrographs of gold nanoparticles and interfering ions on Ami-SiO$_2$.

### 4.2.5 Effect of cyanide ions (CN⁻)

Besides the chloroaurate $[AuCl]^-$, gold-cyanide complex $[Au(CN)_4]^-$ was another commonly found species in the field of gold jewellery and gold-related applications such as mining. This study was aimed to investigate the feasibility of using this substance for the preparation of gold nanoparticles. Au(III) was reacted with excess amount of KCN to form cyanoaurate complexes. The solutions were then adjusted to both pH 3, the optimum condition for the nanogold formation, and pH 10.5 which represented the basic environment commonly found with gold-cyanide complexes. Both solutions were treated with Ami-SiO₂ as described in sections. The residual concentration of Au in the supernatant were analyzed by FAAS.

The conversion of chloroaurate to cyanoaurate complex was verified by UV-Visible spectrophotometry. The $[AuCl_4]^-$ complex normally yields an absorption peak around 314 nm as shown in Figure 4.20. This peak was diminished after the reaction with KCN as the yellow color of $[AuCl_4]^-$ became colorless, thus indicating a complete conversion of gold into $[Au(CN)_4]^-$ at both pH 3 and 10.5.
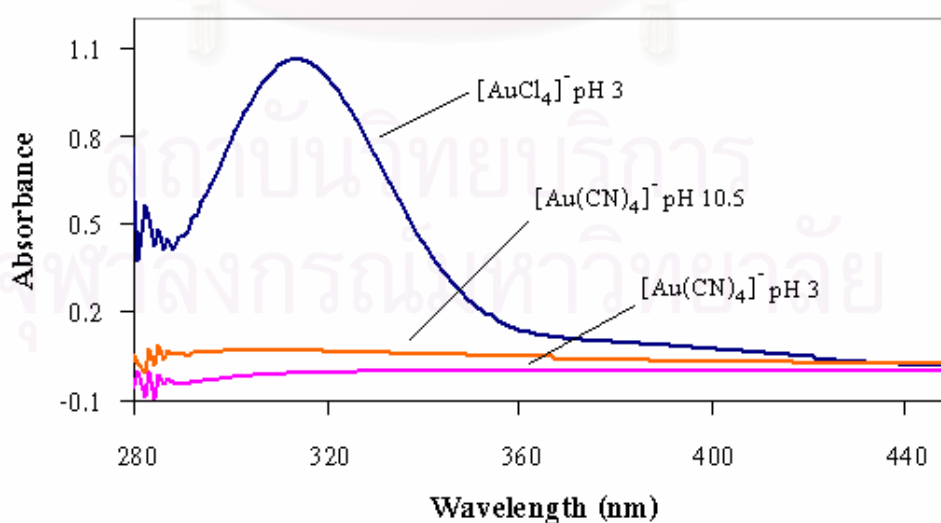


**Figure 4.20** UV-Vis absorption spectra of Au(III) complexes.

After the treatment with Ami-SiO$_2$, no changes on the sorbent were observed. The FAAS analysis in Figure 4.21 revealed that all the gold remained intact in the solution for both pHs.
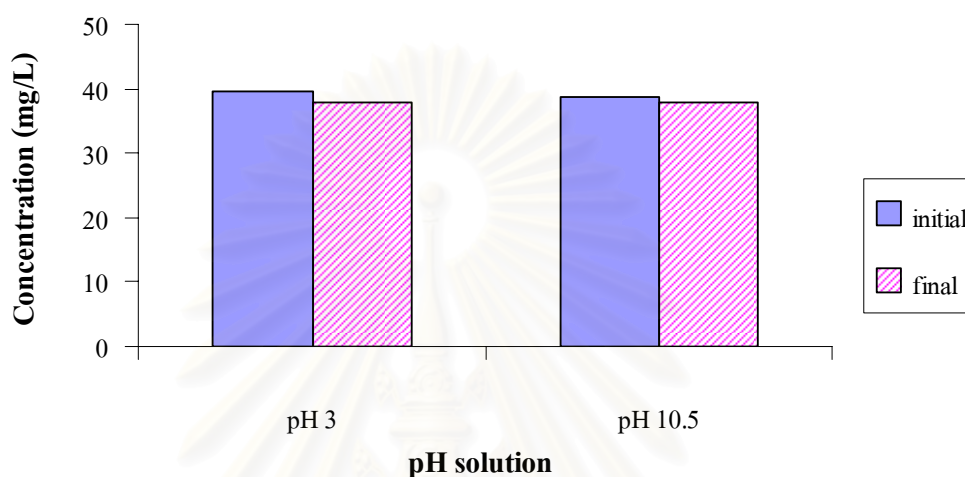


**Figure 4.21** Effect of cyanide ions.

The results indicated that gold were not adsorbed onto the functionalized silica. This can be attributed to the fact that $[Au(CN)_4]^-$ complexes were very stable, as implied by its relatively high stability constant (Log β) and low reduction potential (E$^o$) in table 4.3 [15], and as such were unlikely to undergo neither complexation nor reduction with the amidoxime functional groups on the sorbent.

**Table 4.3** Stability constants and standard reduction potentials for Au(III) complexes

| Complex | Log β | Reduction Reaction | E$^o$ (V) | Ref |
|---------|-------|--------------------|-----------|-----|
| $Au(CN)_4^-$ | ~56 | $Au(CN)_4^- + 3e^- = Au + 4CN^-$ | 0.40 | 15 |
| $AuCl_4^-$ | 26 | $AuCl_4^- + 3e^- = Au + 4Cl^-$ | 1.00 | 15 |

## 4.3  Applications of Ami-SiO$_2$

Ami-SiO$_2$ were evaluated for its potential in the following applications.

### 4.3.1  Recovery of gold on Ami-SiO$_2$

In this study, the amount of gold adsorbed on the Ami-SiO$_2$ were to be recovered and analyzed. The composite nanogold materials obtained from experiment 4.2.1 and 4.2.2 were eluted with 2 mL of aqua regia, brought to the volume (10 mL) and then analyzed by FAAS. The amount of gold adsorbed and released technically represented the extraction and recovery efficiency of the method respectively. The % recovery of gold from the sorbent can then be calculated according to equation (4.3.1-4.3.2)

$$\%R \quad = \quad (D/C) \times 100 \qquad\qquad (4.3.1)$$

$$C \quad = \quad I - F \qquad\qquad (4.3.2)$$

where  D  =  dissolved amount of gold in aqua regia

C  =  calculated amount of gold adsorbed on silica

I  =  initial amount of gold

F  =  residual amount of gold in supernatant

Table 4.4 exhibited the % recovery of Au from the nanogold materials obtained from 40 mg/L Au(III) solutions with varying pH. It was clearly shown that not all of the gold could be recovered in all instances. The best recovery of roughly 86% was achieved with pH 3 solution. Meanwhile, the % recovery of gold from the samples with different initial Au concentrations were displayed in Table 4.5. The lower gold concentrations were noticed to produce more superior % recovery than the higher

ones. Although these numbers are not yet perfect, they can undoubtedly be improved by additional means, e.g. boiling or digestion with acids. Nonetheless, the results firmly pointed to the direction that Ami-SiO$_2$ could very well be used as a decent sorbent for certain applications like gold extraction or preconcentration.

**Table 4.4**   % Recovery of Au on Ami-SiO$_2$ at various initial pH

| pH | % Au Recovery* |
|----|----------------|
| 1  | 41±0.3         |
| 2  | 66±0.4         |
| 3  | 86±0.6         |
| 4  | 79±1.1         |
| 5  | 84±0.7         |
| 6  | 72±1.0         |
| 7  | 78±0.2         |

* Mean value $\pm$ *SD* , n = 3

**Table 4.5**   % Recovery of Au on Ami-SiO$_2$ at various initial concentrations

| Conc. (mgL$^{-1}$) | % Au Recovery* |
|--------------------|----------------|
| 10                 | 97±1.9         |
| 21                 | 91±2.3         |
| 31                 | 87±1.8         |
| 40                 | 86±0.6         |
| 55                 | 76±0.1         |
| 66                 | 74±0.2         |

* Mean value $\pm$ *SD* , n = 3

### 4.3.2 Preparation of gold nanoparticles from jewelry wastewater

This experiment was conducted to demonstrate the feasibility of using wastes, particularly from jewelry or gold-related industries, as a resource of gold for the preparation of gold nanoparticles by the proposed method. The waste sample evaluated was obtained from the precious metal testing lab of the Gem and Jewelry Institute of Thailand. This wastewater basically contained dissolved gold and other precious metal jewelry and its alloying elements as well as various processing materials such as ores, slag, plating solutions, etc. No attempt on the removal of any interfering ions in the waste was made prior to the treatment. The reaction between the waste solution and Ami-SiO$_2$ was effected under the optimal conditions as detailed previously. The resulting solids were characterized by XRF, XRD and TEM.

The XRF spectra of the composite materials prepared from this jewelry wastewater is displayed in Figure 4.22. Apparently other existing major elements including the possible interfering ions, i.e. Ag, Cu, Fe, K, etc., were deposited on the sorbent as well.
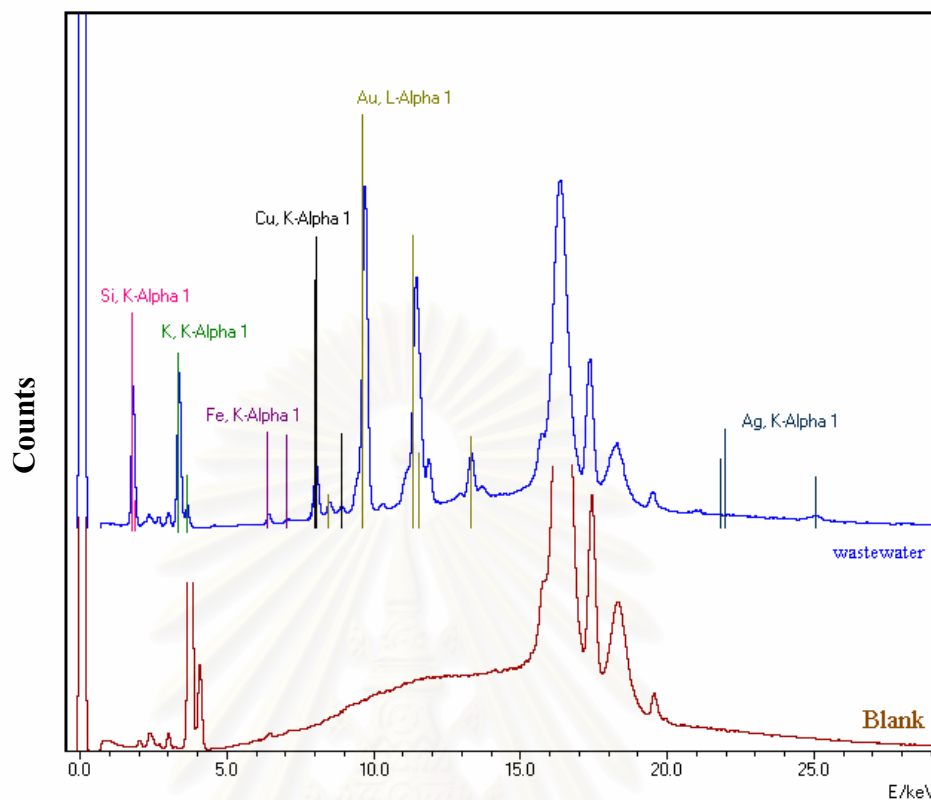
**Figure 4.22** XRF spectra of composite materials prepared from jewelry wastewater.

Nevertheless, the characteristic peaks of gold nanoparticles from XRD analysis (Figure 4.23) were still obtained along with several other unidentified peaks, presumably generated by crystallites of other metals. The particle size of these gold nanoparticles were characterized to be in the range of 100-150 nm as shown by the TEM micrographs in Figure 4.24.
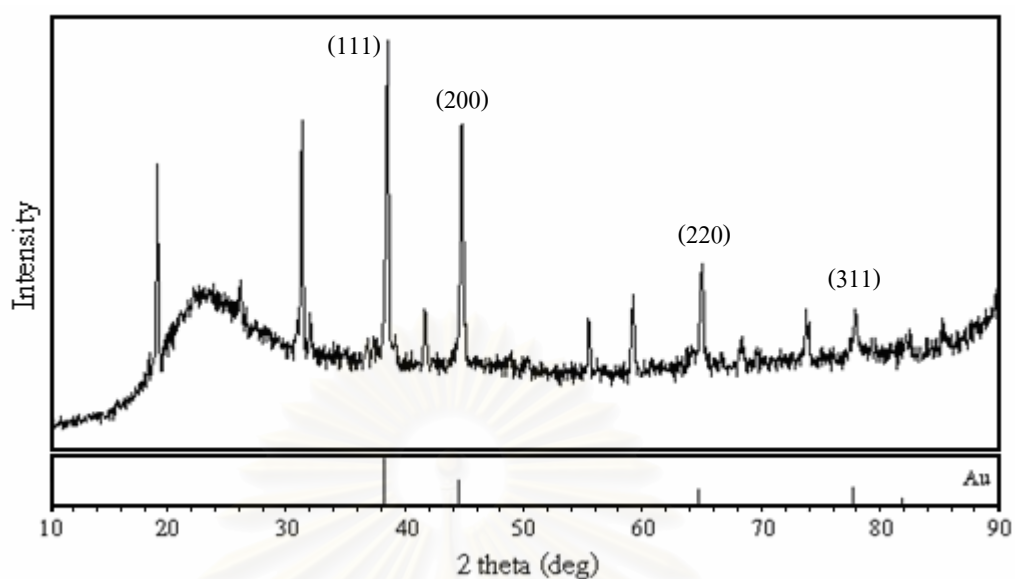
**Figure 4.23** XRD patterns of composite materials prepared from jewelry wastewater.
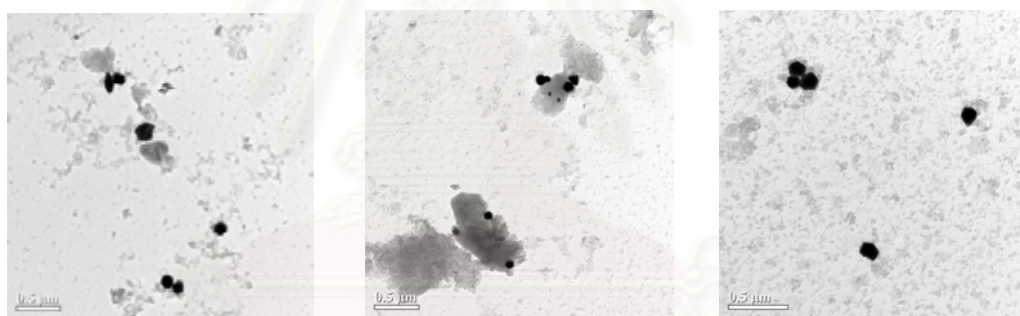


**Figure 4.24** TEM micrographs of composite materials prepared from jewelry

wastewater.

As mentioned above, the XRF and XRD results indicated that other existing metals in the wastewater were also adsorbed on the functionalized silica. These metals could possibly intervene with any potential applications of the prepared gold nanoparticles, therefore, a method of removing these interferences was proposed and evaluated. Four different leaching agents, i.e. 1M HCl, 1M $HNO_3$, 1M $HNO_3$ + $H_2O_2$ and 1M KOH + $H_2O_2$, were used in an effort to scrub these metals out of the sorbent.

Figure 4.25 illustrated XRF spectrum of the composite silica following the treatment with these acids. It was found that by using 1M HCl and 1M $HNO_3$ as leachants, the sorbent were completely liberated from the interfering metals while some still remained but with much lesser magnitude when 1M $HNO_3$ + $H_2O_2$ and 1M KOH + $H_2O_2$ were employed.

After the acid treatments, these particles were characterized by XRD and TEM to verify the existence of gold nanoparticles. The XRD patterns in Figure 4.26 exhibited clean characteristic nanogold peaks for all leachants, thus reassuring the presence of gold nanoparticles. TEM micrographs in Figure 4.27 also revealed that the nanogold particle size remained relatively unchanged.
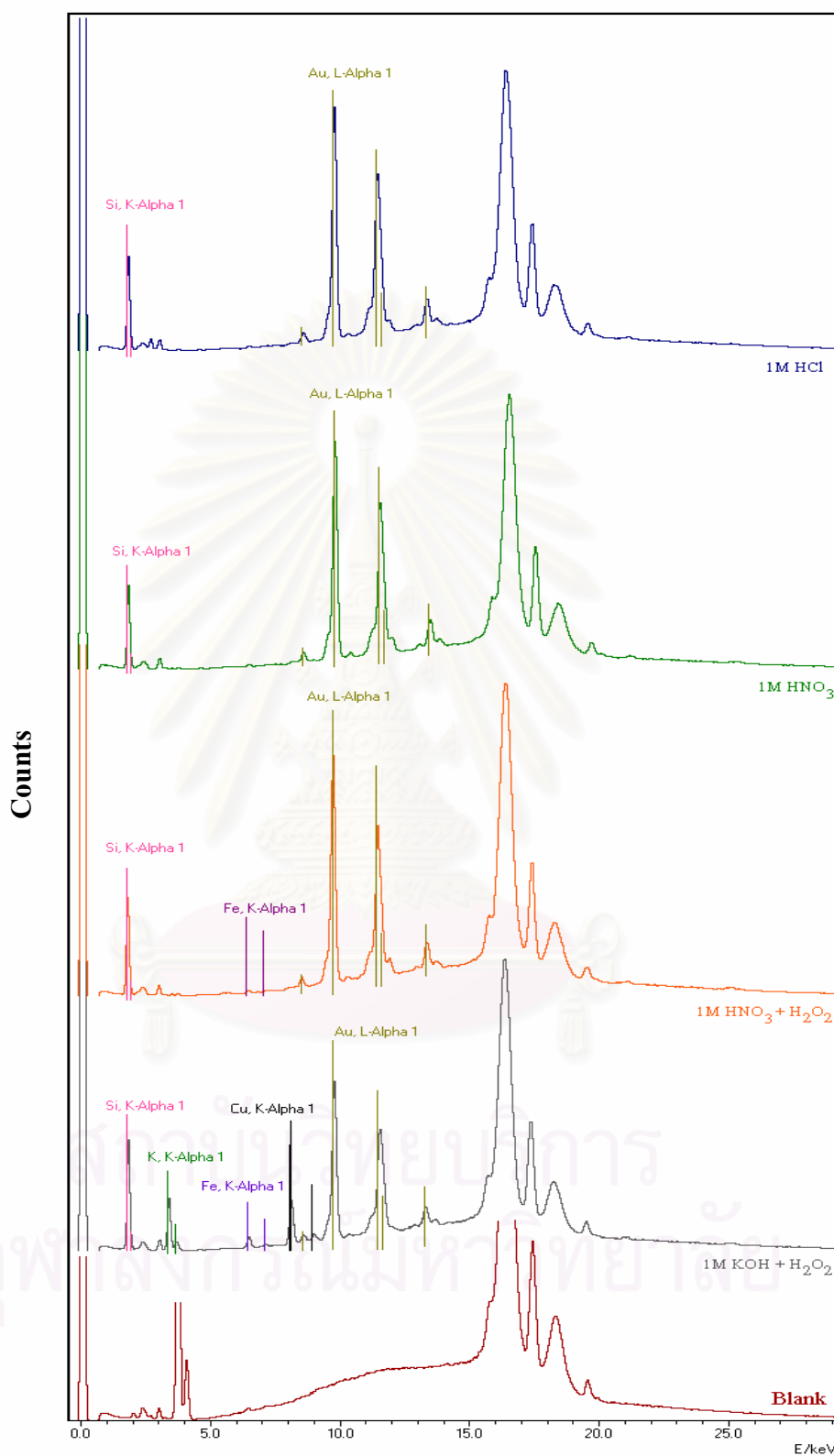
**Figure 4.25** XRF patterns of Au-Ami-SiO$_2$ after leaching with (a) 1M HCl, (b) 1M HNO$_3$, (c) 1M HNO$_3$ + H$_2$O$_2$ and (d) 1M KOH + H$_2$O$_2$.
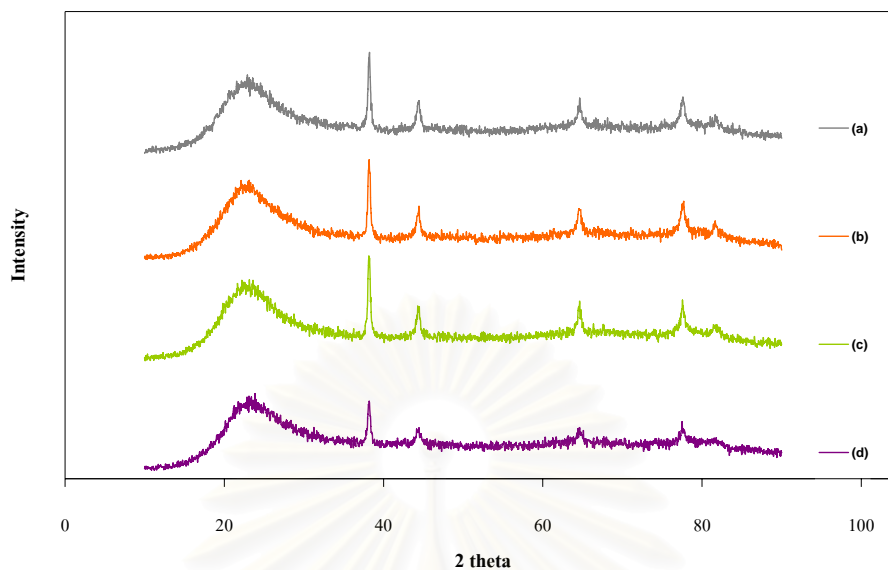
**Figure 4.26** XRD patterns Au-Ami-SiO$_2$ after leaching with (a) 1M HCl, (b) 1M HNO$_3$, (c) 1M HNO$_3$ + H$_2$O$_2$ and (d) 1M KOH + H$_2$O$_2$.
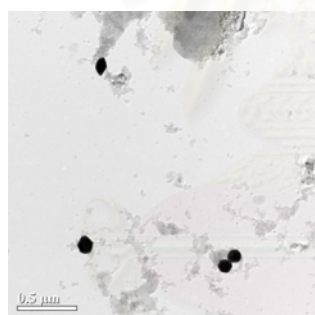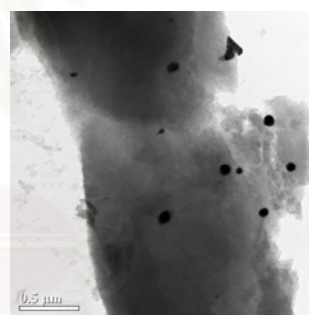


(a) 1M HCl,  124±15 nm       (b) 1M HNO$_3$,  75±15 nm
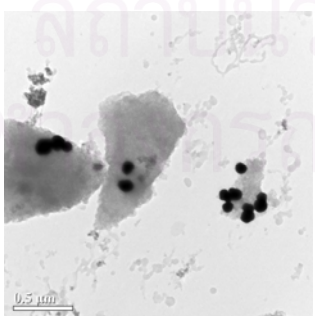
(c) 1M HNO$_3$ + H$_2$O$_2$,  82±12 nm    (d) 1M KOH + H$_2$O$_2$,  70±6.2 nm
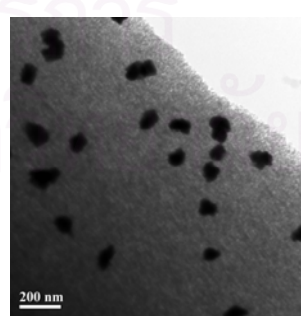
**Figure 4.27** TEM micrographs Au-Ami-SiO$_2$ after leaching with (a) 1M HCl, (b) 1M HNO$_3$, (c) 1M HNO$_3$ + H$_2$O$_2$ and (d) 1M KOH + H$_2$O$_2$.

However, the use of leaching agents as a means to remove interfering metals from the sorbent could present a possibly undesirable aspect as gold might have been eluted or dissolved out of the sorbent as well. To assess the magnitude of this adverse effect, the concentration of gold in the leached solutions were determined and the % Au losses were calculated by equation (4.3.3).

$$\% \text{ Au loss} \quad = \quad (L/C) \times 100 \qquad\qquad (4.3.3)$$

where   L  =  leached gold amount from silica

C  =  calculated amount of gold adsorbed on silica

*The C values were calculated from equation (4.3.2).

It was found that the loss of gold to all of the leaching solutions were relatively minute. The use of 1M $HNO_3$ as a leachant was found optimal in all aspects since it provided apparent interference-free gold nanoparticles with only 2 % of gold loss after leaching, an amount seemingly negligible upon considering its advantages. Hence, the proposed technique proved to be a definite success in the preparation of gold nanoparticles from the jewelry wastewater.

**Table 4.6**   % Au loss from Ami-$SiO_2$

| Leachant | % Au loss |
|----------|-----------|
| 1M HCl | 3.03 |
| 1M $HNO_3$ | 2.06 |
| 1M $HNO_3$ + $H_2O_2$ | 1.84 |
| 1M KOH + $H_2O_2$ | 3.07 |

# CHAPTER V

# CONCLUSION

The functionalized silica was prepared by a 3-step on-solid-phase synthesis; (i) aminopropylation (AP-SiO$_2$), (ii) cyanoamidation (CA-SiO$_2$) and (iii) amidoximation (Ami-SiO$_2$). The resulting phase was characterized by 13-Carbon nuclear magnetic resonance spectrometer ($^{13}$C-NMR), Fourier transform infrared spectroscopy (FT-IR), elemental analysis (EA) and thermal gravimetric analysis (TGA). The results of characterization from each systhesis step indicated that the synthesis was successful. The reductive capacity of Ami-SiO$_2$ was determined by redox titration method with KMnO$_4$ solution and found to be 1.6±0.1 mEq/g Ami-SiO$_2$.

The optimum conditions for the preparation of gold nanoparticles were investigated e.g. solution pH, contact time and concentration of [AuCl$_4$]$^-$. The obtained gold nanoparticles were characterized by X-ray diffractometry (XRD), diffuse reflectance ultraviolet visible spectrophotometry (DR-UV-Vis), X-ray fluorescence spectrometry (XRF) and transmission electron microscopy (TEM). The nanogold preparation from [AuCl$_4$]$^-$ solution was optimized at pH 3 and 30 minutes of contact time. The maximum capacity of Ami-SiO$_2$ was 39±0.1 mg Au/g Ami-SiO$_2$. Moreover, Ami-SiO$_2$ can adsorb other metal ions (Ag$^+$, Cu$^{2+}$, Ni$^{2+}$ and Zn$^{2+}$) as well. The gold particles obtained from all experiments were in nanoscale.

Two practical applications, the recovery of gold and the preparation of nanogold from jewelry waste, by Ami-SiO$_2$ were evaluated. The functionalized silica proved to be a success in both instances.

## Suggestions for future work

Gold nanoparticles obtained from this study posses a distinct advantage in that they are stabilized on a very durable material (i.e. silica), therefore, its application as a catalyst for reactions under aggressive conditions, e.g. high mechanical movement or high temperature, might be of interest. There are also some aspects that can be improved for the proposed technique such as its applicability to $[Au(CN)_4]^-$ or the effect of anions to the nanogold formation that might be worth studying as well.
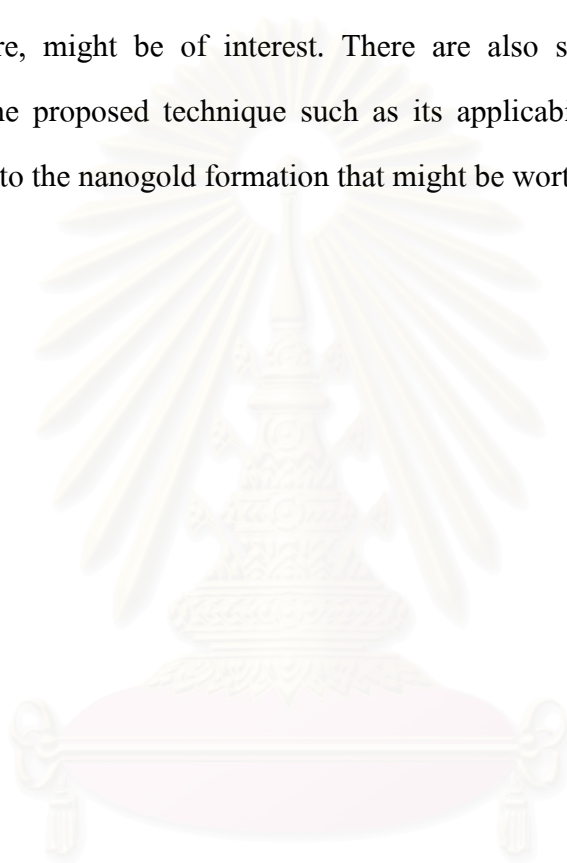
# REFERENCES

[1]   Goldipedia [online]. CFP Group. Available from: http://www.goldipedia.gold. org/[2008, March 24].

[2]   Nano-gold in anti-angiogenic therapy [online]. Mukhopadhyay. Avialable from: http://mayoresearch.mayo.edu/mayo/research/dev_lab/nanogold.cfm[2008, March 24].

[3]   Raj, C. R.; Abdelrahman, A. I.; and Ohsaka, T. Gold nanoparticle assisted electroreduction of oxygen. Electrochemistry Communication 7 (2005): 888-893.

[4]   Bandyopadhyay, M.; et al. Gold nano-particles stabilized in mesoporous MCM-48 as active CO-oxidation catalyst. Microporous and Mesoporous Materials 89 (2006): 158-163.

[5]   Processes for refining gold jewelry scraps and waste [online]. Corti, C. W. Avialable from: http://www.ganoksin.com/borisat/nenam/ajm-roads-2-recove ry.htm[2008, March 24].

[6]   Lin, E.; Lu, Y.; and Zeng H. Extraction of gold from Au(III) ion containing solution by a reactive fiber. Journal of Applied Polymer Science. 49 (1993): 1635-1638.

[7]   Puddephatt, R. J.; and Vittal, J. J. Gold: inorganic & coordinate chemistry. Encyclopedia of Inorganic Chemistry. Chichester UK: John Wiley & Sons, (1994): 1320-1331.

[8]   Bailar, L. C.; Emeleus, H. J.; Nyholm, R.; and Trotman-Dickenson, A. F. Comprehensive Inorganic Chemistry. Vol. 3 and 4. Oxford, England: Pergamon, (1973).

[9]   Grigor'eva, T. A.; and Sukneva, L. S. Effect of sulfur, antimony trisulfide and arsenic trisulfide on gold solubility. Geokhimiya 10 (1981): 1534-154.

[10] Read, H. H. Rutley's Elements of Mineralogy. 26th Edition. London: Thomas Murby, (1970).

[11] Liu, H. B.; Ascencio, J. A.; Perez-Alvarez, M.; and Yacaman, M. Journal Surface Science 491 (2001): 88.

[12] Dick, K.; Dhanasekaran, T.; Xhang, Z.; and Misel, D. Journal of the American Chemical Society 124(10) (2002): 2312.

[13] Cortie, M.; and Lingen, E. V. D. Gold 2003. Vancouver: 28th September – 1st October 2003.

[14] Greenwood, N. N.; and Earnshaw, A. Chemistry of the elements. UK: Butterworth-Heinemann, (1997).

[15] Nicol, M. J.; Fleming, C. A.; and Paul, R. L. The chemistry of the extraction of gold. The Extraction Metallurgy of Gold in South Africa. Vol. 2. Stanley: G. G., (1987): 831-905.

[16] Hiskey, J. B.; and Atluri, V. P. Dissolution chemistry of gold and silver in driferrent lixiviants. Mineral Process Extraction Metallic Rev. 4 (1988): 95-134.

[17] Webster, J. G. The solubility of gold and silver in the system gold-silver-sulfur-oxygen-water at $25^{o}$C and 1 atm. Geochimica et Cosmochimica Acta 50(9) (1986): 1837-1845.

[18] Skibsted, L. H.; and Bjerrum, J. Studies on gold complexes. I. Robustness stability and acid dissolution of the tetramminegold(III) ions. Acta Chem. Scand. A28(7) (1974a): 740-746.

[19] Skibsted, L. H.; and Bjerrum, J. Studies on gold complexes. II. The equilidrium between gold(I)and gold(III) in the ammonia system and the standard potentials of the couples involving gold, diamminegold(I) and tetramminegold(III) ions. Acta Chemica Scandinavica A28(7) (1974b): 764-770.

[20] Pal, A.; Pal, T.; Stokes, D. L.; and Vo-Dinh, T. Photochemically prepared gold nanoparticles: A substrate for surface <u>Current Science</u> 84 (2003): 1342-1345.

[21] Patungwasa, W.; and Hodak, J. H. pH tunable morphology of the gold nanoparticles produced by citrate reduction. <u>Materials Chemistry and Physics</u>. 108 (2008): 45-54.

[22] Mandal, S.; et al. Synthesis of a stable gold hydrosol by the reduction of chloroaurate ions by the amino acid, aspartic acid. <u>Indian Academic Science (Chemical Science)</u> 114 (2002): 513-520.

[23] Stremsdoerfer, G.; et al. Autocatalytic deposition of gold and palladium onto n-GaAs in acidic media. <u>Journal of the Electrochemical Society</u> 135 (1988): 2881-2886.

[24] Turkevitch, J.; and Stevenson, P. C.; Hillier, J. Nucleation and growth process in the synthesis of colloidal gold. <u>Discussions of the Faraday Society</u> 11 (1951): 55-75.

[25] Yonezawa, T.; and Kunitake, T. Practical preparation of anionic mercapto ligand stabilized gold nanoparticles and their immobilization. <u>Colloids Surface A: Physicochemical and Engineering Aspects</u> 149 (1999): 193-199.

[26] Brust, M.; et al. Synthesis of Thiol-derivatised Gold Nanoparticles in a Two-Phase Liquid-Liquid System. <u>Journal of the Chemical Society, Chemical Communications</u> (1994): 801-802.

[27] Brust, M.; et al. Synthesis and Reactions of Functionalised Gold Nanoparticles. <u>Journal of the Chemical Society, Chemical Communications</u> (1995): 1655-1656.

[28] Moriguchi, I.; et al. Synthesis of gold particles in organized molecular assembly films. <u>Colloids Surface A: Physicochemical and Engineering Aspects</u> 126 (1997): 159-166.

[29] Hermanson, K. D.; et al. Dielectrophoretic Assembly of Electrically Functional Microwires from Nanoparticle Suspensions. <u>Science</u> 294 (2001): 1082-1086.

[30] Corti, C. W.; and Holliday, R. J. Commercial aspects of gold applications: from materials science to chemical science. Gold Bull 37 (2004): 1-2.

[31] Hao, Z.; Guo, Z. Y. and Liang, Y. Support Supported gold catalysts used for ozone decomposition and simultaneous elimination of ozone and carbon monoxide at ambient temperature. Applied Catalysis B: Environmental 33 (2001): 217-222.

[32] Wilson, M.; et al. Nanotechnology-basic science and emerging technologies. Chapman Hall (2002).

[33] Iwakoshi, A.; Nanke, T.; and Kobayashi, T. Coating materials containing gold nanoparticles. Proceedings of the International Conference 'Gold2003: New Industrial Application for Gold Vancouver, Canada: [2003].

[34] Christian, G. D. and O'Reilly, J. E. Instrument Analysis. Vol. 2. (n.d.): Allyn and Bacon, 1986.

[35] Catalytic Synthesis of carbon Nanotubes [online]. (n.d.). Avialable from: http://cobweb.ecn.purdue.edu/~catalyst/Carbon%20Nanotubes/Catalytic%20Nanotubes/Catalytic%20Synthesis%20of%20Carbon%20Nanotubes.htm [2008, March 24].

[36] X-ray powder Diffractometer [online]. (n.d.). Avialable from: http://www.tint.or.th/adv/phys_oap/XRD.pdf[2008, March 24].

[37] Jin, Y.; Wang, P.; and Yin, D.; et. al. Gold nanoparticles prepared by sonochemical method in thiol-functionalized ionic liquid. Colloids Surface A: Physicochemical and Engineering Aspects 302 (2007): 366-370.

[38] Glomm, W. R.; et al. Functionalized gold nanoparticles for application in biotechnology. Journal of Dispersion Science and Technology 26 (2005): 389-414.

[39] Yang, Y. C.; Wang, C. H.; Hwu, Y. K.; and Je, J. H. Synchrotron X-ray synthesis of colloidal gold particles for drug delivery. Materials Chemistry and Physics 100 (2006): 72-76.

[40] Ghosh, A.; et al. Preparation and stabilization of gold nanoparticles formed by in situ reduction of aqueous chloroaurate ions within surface modified mesoporous silica. Microporous and Mesoporous Materials 58 (2003): 201-211.

[41] Ivanova, S.; Petit, C.; and Pitchon, V. A new preparation method for the formation of gold nanoparticles on an oxide support. Applied Catalysis A 267 (2004): 191-201.

[42] Paek, S. M.; Jang, J. U.; Hwang, S. J.; and Choy, J. H. Exfoliation-restacking route to Au nanoparticle-clay nanohybrids. Journal of Physics and Chemistry of Solid 67 (2006): 1020-1023.

[43] Evangelista, S. M.; DeOliveira, E.; Castro, G. R.; Zara, L. F.; and Prado, A. G. S. Hexagonal mesoporous silica modified with 2-mercaptothiazoline for removing mercury from water solution. Surface Science 601 (2007): 2194-2202.

[44] Padilha, P. M.; Gomes, L. A. D.; Padilha, C. C. F.; Moreir, J.C.; and Dias Filho, N. L. Determination of metal ions in natural waters by flame-AAS after preconcentration on a 5-Amino-1,3,4-thiadiazole-2-thiol modified silica gel. Analytical Letters 32 (1999): 1807.

[45] Fan, J.; et al. Preparation of the diphenylcarbazone-functionalized silica gel and its application to on-line selective solid-phase extraction and determination of mercury by flow-injection spectrophotometry. Journal of Hazardous Materials 150 (2008): 343-350.

[46] Xie, F.; Lin, X.; Wu, X.; and Xie, Z. Solid phase extraction of lead(II), copper(II), cadmium(II) and nickel(II) using gallic acid-modified silica gel

prior to determination by flame atomic absorption spectrometry. <u>Talanta</u> 74 (2008): 836-843.

[47] Ngeontae, W. <u>Synthesis of chemically modified silica gel for preconcentration of heavy metals</u>. Doctoral dissertation analytical chemistry science Chulalongkorn University, 2550.

[48] ศุภชัย ใช้เทียมวงศ์. <u>ปฏิบัติการเคมีปริมาณวิเคราะห์</u>. พิมพ์ครั้งที่ 6. กรุงเทพฯ: สำนักพิมพ์จุฬาลงกรณ์มหาวิทยาลัย, 2543.

[49] <u>Molarity</u> [online]. Barbalace, R. C. Avialable from: http://environmental chemistry.com/yogi/chemistry/MolarityMolalityNormality.html[2008, February 28].

[50] Farges, F.; Sharps, J. A.; and Brown Jr, G. E. Local environment around gold(III) in aqueous chloride solutions: an EXAFS spectroscopy study. <u>Geochimica et Cosmochimica Acta.</u>, 57 (1992): 1243-1252.

[51] Khanna, P. K.; Gokhale, R.; and Subbarao, V. V. V. S.; et. al. PVA stabilized gold nanoparticles by use of unexplored albeit conventional reducing agent. <u>Materials Chemistry and Physics.</u>, 92 (2005): 229-233.

[52] Aslam, M.; et al. Novel one-step synthesis of amine-stabilized aqueous colloidal gold nanoparticles. <u>Journal of Materials Chemistry</u> 14 (2004): 1795-1797.

[53] Lutfor, M. R.; Silong, S.; Yunus, W. M. Z. W.; Rahman, M. Z. A.; Ahmad, M.;and Haron, J. Polymer bearing amidoxime groups for extraction of arsenic from aqueous media [Online]. (1997). Available from: http://www.eng-consult.com/BEN/papers/Paper-lutfor.PDF[2008, February 28].

[54] Voloschik, I. N.; Litvina, M. L.; and Rudenko, B. A. Separation of transition and heavy metals on an amidoxime complexing sorbent. <u>Journal of Chromatography A</u> 671 (1994): 51-54.

[55]  Devi, P.; Gangaiah, T.; and Naidu, G. P. K. Determination of trace metals in water by neutron activation analysis after preconcentration on a poly(acrylamidoxime) resin. <u>Analytica Chimica Acta</u> 249 (1991): 533-537.

[56]  Lide, D. R. <u>CRC handbook of chemistry and physics</u>. London: Taylor & Francis Group, 2008.

# VITA

Miss Nutpatsa Sirikanjanawanit was born on April 15, 1983 in Bangkok, Thailand. She received her Bachelor degree of Science in Chemistry from Srinakharinwirot University in 2005. After that, she has been a graduate student at the Department of Chemistry Chulalongkorn University and a member of Environmental Analysis Research Unit. She finished her postgraduate study with the Master degree of Science in 2008. The present address is 728 Soi Onnuch 16, Onnuch Road, Sounloung, Bangkok, Thailand, 10250. Contact number is 085-9663510.